Journal of Structural Geology 96 (2017) 35–53

Contents lists available at ScienceDirect

Journal of Structural Geology

journal homepage: www.elsevier.com/locate/jsg

Active inversion tectonics, simple shear folding and back-thrusting at Rioni Basin, Georgia

A. Tibaldi [a, *], V. Alania [b], F.L. Bonali [a], O. Enukidze [b], N. Tsereteli [b], N. Kvavadze [b], O. Varazanashvili [b]

[a] University of Milan Bicocca, Milan, Italy
[b] M. Nodia Institute of Geophysics, M. Javakhishvili Tbilisi State University, Georgia

ARTICLE INFO

Article history:
Received 29 July 2016
Received in revised form
19 December 2016
Accepted 23 January 2017
Available online 27 January 2017

Keywords:
Caucasus
Active faults
Simple shear folds
Seismicity
Inversion tectonics
Backthrusts

ABSTRACT

The Rioni Basin, located between the Greater and Lesser Caucasus in Georgia, is an outstanding example of ongoing inversion tectonics. Marine and continental deposits of Cretaceous-Neogene age have been locally uplifted since the end of Miocene. The uplifted area totals 1300 km^2, and Plio-Quaternary river deposits have been raised up to 200 m above the surrounding plains. Inversion tectonics has been accompanied by the development of south-vergent asymmetrical folds and strike-slip faults along the border of the uplifted area. The folds have locally an en-échelon geometry and microtectonic data indicate rotation of the paleostress direction over time, suggesting simple shear deformation. In the interiors of the uplifted area, there are gentle symmetrical folds and one main active south-dipping reverse fault, corresponding to a backthrust. Morphostructural evidence, as well as the tilting of Quaternary strata, the offset of Quaternary alluvial deposits and the presence of crustal seismic activity, indicate that compressional tectonics is still active. The combination of field data with seismic reflection sections shows that inversion tectonics took place through a series of north-dipping blind thrusts and a wedge with passive back-thrusting. Uplift and contraction are more developed along the eastern part of the study area, suggesting the westward propagation of the closure of the Transcaucasian depression.

1. Introduction

The Caucasus is a young orogenic system that started to develop following the Tertiary collision between the Arabian and Eurasian plates. The collision caused the partial closure of previous basins whose modern remnants are represented by the Black Sea and the Caspian Sea (Fig. 1). Between these two depressions are the Greater and Lesser Caucasus, separated by the Transcaucasian intermontane valley. In the Transcaucasian depression, during Oligocene-Early Miocene times, the Rioni Basin and the Kura Basin developed as foreland depressions, and later on were involved into the orogenic fold-and-thrust belts (Adamia et al., 1977, 2010, 2011a, 2011b; Banks et al., 1997; Mosar et al., 2010; Sosson et al., 2010, 2013; Forte et al., 2010; Alania et al., 2016).

The recent geodynamic processes are also attested by magmatic activity, with volcanoes emplaced both at the edge of the Greater Caucasus, such as Mt Elbrus, or across the Lesser Caucasus (Rebai et al., 1993; Pasquaré et al., 2011). The volcanism in the mountain belt, associated to the Eurasian and Arabian plates collision, started only in late Miocene in the central sector of the Caucasus (Adamia et al., 1977, 2017; Koronovskii and Demina, 1999).

Recent GPS data and plate tectonic models indicate that, also at present, the Greater and Lesser Caucasus are tectonically very active, with ongoing mountain building processes comprising complex plate boundary interactions with vertical and horizontal strain partitioning (Rebai et al., 1993; Koçyiğit et al., 2001; Reilinger et al., 2006; Tan and Taymaz, 2006; Kadirov et al., 2013). Very active ongoing processes of mountain building are also demonstrated by the diffuse seismicity with compressional events of magnitude up to 7 (Tsereteli et al., 2016).

All these data indicate that the Caucasus orogens and the Transcaucasus depression represent outstanding examples of recent mountain building processes of Neogene-Quaternary times. The Neogene compression produced the partial closure of the Eastern Black Sea and the consequent flexure of its northern margin (Banks et al., 1997). This flexuring, in turn, induced the formation of

* Corresponding author.
E-mail address: alessandro.tibaldi@unimib.it (A. Tibaldi).

http://dx.doi.org/10.1016/j.jsg.2017.01.005
0191-8141/

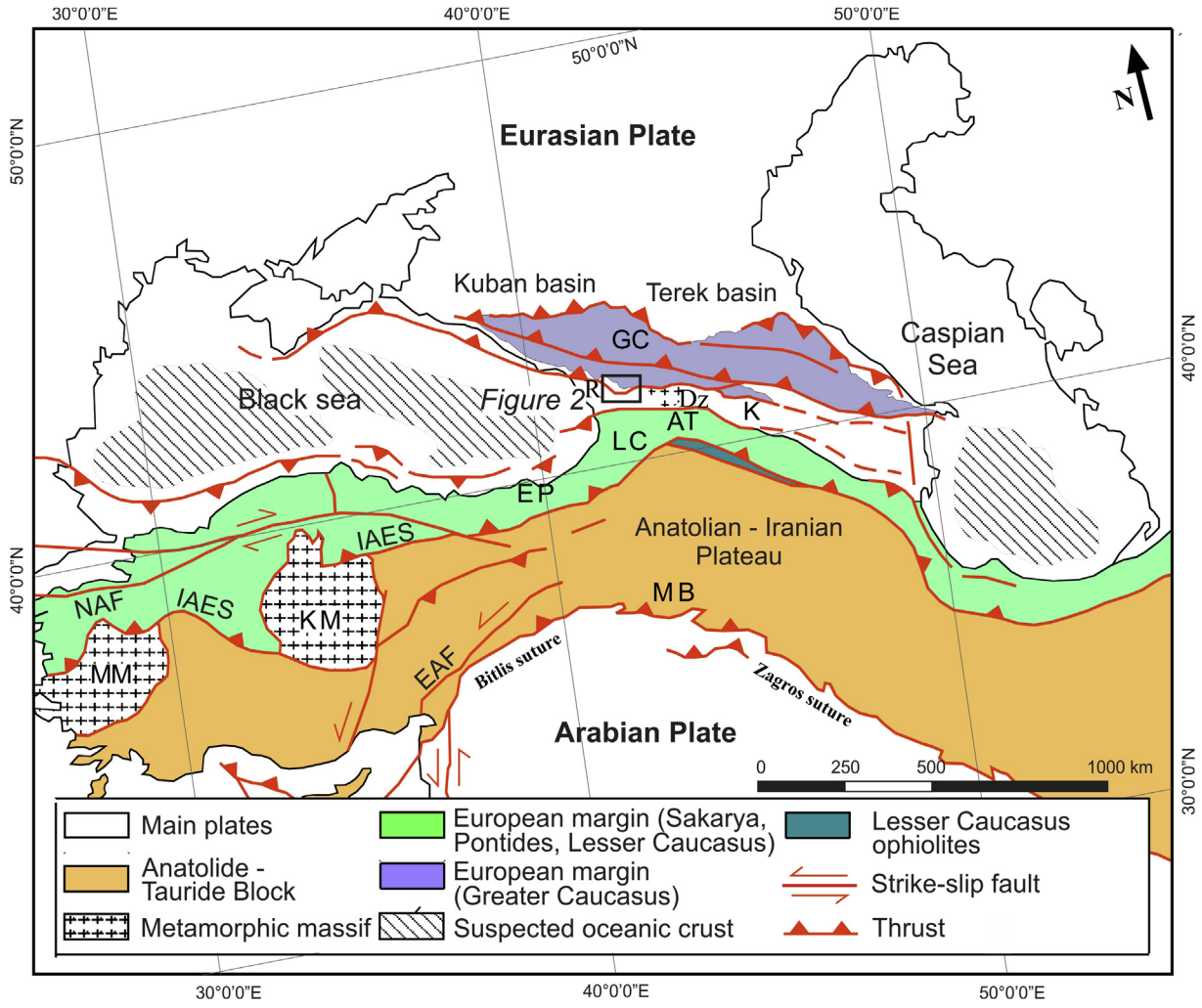

Fig. 1. Tectonic map of the Arabia - Eurasia collision zone (modified from Sosson et al., 2010). Abbreviations: GC-Greater Caucasus; LC-Lesser Caucasus; AT-Achara-Trialeti; R-Rioni; Dz-Dzirula; K-Kura; MB-Mus Basin; EP-Eastern Pontides; KM-Kirsehir Massif; EAF-Eastern Anatolian Fault; NAF-North Anatolian Fault; IAES-Izmir-Ankara-Erzincan Suture; MM-Menderes Massif.

the relatively small Rioni Basin, which is normally interpreted as a foreland basin filled with late Miocene to Quaternary sediments. Despite this structural setting, the Rioni Basin also displays a series of folds that suggest inversion tectonics. Therefore, we undertook a major effort to understand the age and mechanisms of this inversion tectonics, also taking in consideration the potential associated seismic hazard in case of still-ongoing processes. The region, in fact, hosts several villages and small towns and an important hydroelectric infrastructure. We thus integrated new field geological-structural, microtectonic and geomorphological data with seismological data and seismic reflection sections, in order to describe the structural architecture of the Rioni Basin. Regional observations have been integrated with detailed and systematic microtectonic data with the aim of understanding the development of the shallow folds and reconstructing the evolution of stress orientations. The results show that most of the uplifting Rioni Basin is bounded by south-vergent hidden thrusts, whereas to the east it is limited at the surface by simple shear folds. The interiors of the uplifting area are affected by a main active back-thrust in response to a tectonic wedge. The data provided here are helpful not only for a better understanding of the structural architecture and seismic hazard of the area, but also as a general example of how active blind thrusts and shallow faults may influence surface structures and landforms.

2. Geological settings

2.1. Regional geology

The Rioni Basin is located between the western Greater Caucasus orogen and the Achara-Trialeti fold and thrust belt, which belongs to the northern part of Lesser Caucasus (Fig. 1). The western Greater Caucasus is predominantly a single-vergent orogeny (i.e. southward), in contrast to the central and eastern parts of Greater Caucasus that show a double-vergent orogenic wedge (Forte et al., 2014). During the long Neotethys subduction process, several domains formed in back-arc locations within the Eurasian Plate, most notably the Greater Caucasus basin that opened up in Early–Middle Jurassic (Khain, 1974; Dercourt et al., 1986; Adamia et al., 1981, 2011a), and the western and eastern Black Sea basins that opened up during the Cretaceous and Cenozoic (Adamia et al., 1974; 1981; Letouzey et al., 1977; Finetti et al., 1988; Zonenshain and Le Pichon, 1986; Okay et al., 1994, 2013; Robinson et al., 1996; Spadini et al., 1996; Cloetingh et al., 2003; Vincent et al., 2005; Yegorova and Gobarenko, 2010; Khriachtchevskaia et al., 2010; Stephenson and Schellart, 2010) or Middle Jurassic-Early Cretaceous (Sosson et al., 2016). Based on apatite fission-track data, the exhumation process in the Greater Caucasus started in the Oligocene and reached

the highest rate in the Miocene-Pliocene (Vincent et al., 2007, 2011; Avdeev and Niemi, 2011). Plate reorganization occurred within the Arabia-Eurasia collision zone at ~5 Ma BP, and first-order plate motions have remained relatively constant since that time (Westaway, 1994; McQuarrie et al., 2003; Allen et al., 2004). The period ~3–5 Ma coincides with the formation of the Zagros fold and thrust belt, the South Caspian Sea and Rioni-Kura foreland fold and thrust belts (Adamia et al., 2010, 2011a; Forte et al., 2010; Devlin et al., 1999). Apatite fission-track data from the central part of Achara-Trialeti fold and thrust belt (Borjomi area) indicate that exhumation of Paleogene strata and compressional deformation started in the Middle Miocene (Albino et al., 2014). According to GPS data, the convergence rate between the Greater Caucasus and Lesser Caucasus increases from West to East in the Caucasus region; namely, the convergence rate in the Rioni basin is about 4 mm/yr, and in Kura foreland (in Azerbaijan) it is about 14 mm/yr (Reilinger et al., 2006).

The Rioni Basin developed mainly during the Oligocene-Miocene through loading by the Achara-Trialeti and Greater Caucasus fold and thrust belts (Banks et al., 1997). The northern part of the Rioni foreland is characterized by thrusts with a curved geometry in plan view, and is dominated by a thin-skinned tectonic style (Banks et al., 1997; Adamia et al., 2010, 2011b). Ramp anticlines formed above south-vergent thrusts that detach and flatten along the Upper Jurassic evaporites of the Rioni foreland basin. The anticlines involve Cretaceous-Neogene strata and are arranged in an en-échelon pattern. These structures are clearly related to compression in the Greater Caucasus (Banks et al., 1997; Adamia et al., 2010). Regionally, the Greater Caucasus frontal folds began forming as early as Late Eocene, but the anticlines of the northern part of Rioni Basin apparently formed from the Middle Miocene onwards; most of their growth probably took place during the Meotian, whereas there was very little growth during the Pontian-Recent (Banks et al., 1997). Beneath the ramp anticlines and a similar offshore structure, known as Shatsky Ridge, it can be noticed that the top Cretaceous regional surface actually falls by seismic profile across the compressional faults. This suggests that the thrusts overlie earlier extensional faults that are likely to be related to the opening of the Eastern Black Sea. As a consequence, these normal faults should have a Late Paleocene to Early Eocene age (Robinson et al., 1996; Banks et al., 1997).

The frontal folds of the Achara-Trialeti fold and thrust belt form the oil-bearing structures along the southern flank of the Rioni basin. These structures are compressional ramp anticlines formed initially from the Early Sarmatian to the Pontian with minor growth continuing through the Quaternary (Banks et al., 1997; Adamia et al., 2010).

2.2. Stratigraphy of the Rioni Basin

The distribution of the main stratigraphic units of the Rioni Basin is shown in the geological map of Fig. 2 and schematized in the stratigraphic column of Fig. 3. The sedimentary cover of the Rioni basin is commonly >5 km thick (Adamia et al., 2011a). The oldest formation exposed north (Greater Caucasus) of the Rioni Basin is represented by Lower Jurassic (about 1500 m thick) sandstones and shales. The pre-Jurassic basement crops out in the Dzirula Massif that separates the Rioni and Kura basins. The Dzirula massif is dominated by pre-Variscan diorite-plagiogneiss-migmatite complexes and Variscan granitoids (Zakariadze et al., 2007; Adamia et al., 2011a). Mid-Jurassic deposits are represented by Bajocian tuff-turbidities with rare bands of calk-alkaline andesite-basalts and Bathonian, freshwater-lacustrine, coal-bearing and sandy-argillaceous rocks; the thickness is about 2500 m. Upper Jurassic rocks are evaporites, clastic deposits, and basalts (about 500 m thick). Lower Cretaceous turbidities, dolomites, limestones (Urgonian facies), organogenic limestones and marls, and conglomerates at the base, rest transgressively on the Upper Jurassic rocks; their thickness is about 350–400 m (Adamia et al., 2011a). Within the Rioni Basin and in the surrounding area, there are also Upper Cretaceous, Paleocene and Eocene deposits mainly made of neritic organogenic limestones, marls and volcanogenic rocks; their thickness in some places exceeds 2000 m (Adamia et al., 2011a). The Oligocene-Lower Miocene (Maykopian) series is mainly represented by alternating gypsiferous clays and sandstones that are highly specific for the Eastern Paratethys; their thickness is about 800–900 m (Banks et al., 1997; Jones and Simmons, 1997; Adamia et al., 2010).

Syntectonic strata from the Middle - Upper Miocene (Sarmatian and Meotian-Pontian), Pliocene (Cimmerian and Kuyalnikian) and Pleistocene (Gurian) are represented by shallow marine and continental, predominantly terrigenic clastic deposits, conglomerates, sandstones, mudstones, claystones, sandy clays, clays and rare shell-beds. The total thickness of the syntectonic strata is about 1500–2000 m (Banks et al., 1997; Adamia et al., 2010).

3. New data

In the next sections we illustrate the results of multidisciplinary analyses we conducted in the region. We firstly describe our geomorphological observations, then we provide field geological-structural data, seismological data, and seismic reflection profiles.

3.1. Geomorphology

Part of the Rioni Basin presents geomorphological characteristics that are worthy of attention. While along the coast of Black Sea and towards the Lesser Caucasus, the floor of the Rioni Basin is flat (altitudes mostly < 10 m a.s.l.), more to the north, in the area shown in Fig. 4, the topography rises up to 300–400 m a.s.l. This area is characterized by a complex morphology with deeply dissected alluvial fans and series of rivers terraces placed at different altitudes. Elongated features are also present and correspond to anticline structures, as described in the structural geology section.

Most of this relatively high area is covered by fluvial conglomerates of Pliocene-Quaternary age. These conglomerates have been found up to altitudes of 350–400 m (Fig. 5A–B) and thus stand 100–200 m above the surrounding valley floor. The conglomerate succession, in turn, is deeply incised by the present-day Enguri river: For instance, at the foothill of the Greater Caucasus, immediately south of the Enguri dam, the river is deeply entrenched in a canyon, with the river bed located at 305–290 m a.s.l. (Fig. 5A). This canyon has been cut into the carbonatic bedrock, leaving a river terrace with conglomerates at an altitude of 409–395 m a.s.l. Another parallel river, located more to the east, also excavated a 140–600 m deep gorge into the same bedrock. Further south, the northern segment of the Enguri river flows at an altitude of 255–240 m a.s.l.; along the same course segment, the conglomerates in the upper terraces stand up to 370 m a.s.l., indicating an erosion of about 120 m. At the foothill of the Greater Caucasus there are also two large alluvial fans (Fig. 4). They show deep river incisions and are, in turn, cut by more recent terraces, especially to the west.

River terraces are particularly developed along the Enguri valley, in the westernmost part of the elevated area. Most, if not all, are asymmetric terraces, in that they developed only along the eastern side of the river valley. As an example, in Fig. 6A shows the strong asymmetry of the river terraces produced by the Enguri river. In the background of this oblique view of the area (looking north), it is possible to observe that at least eight orders of river terraces are

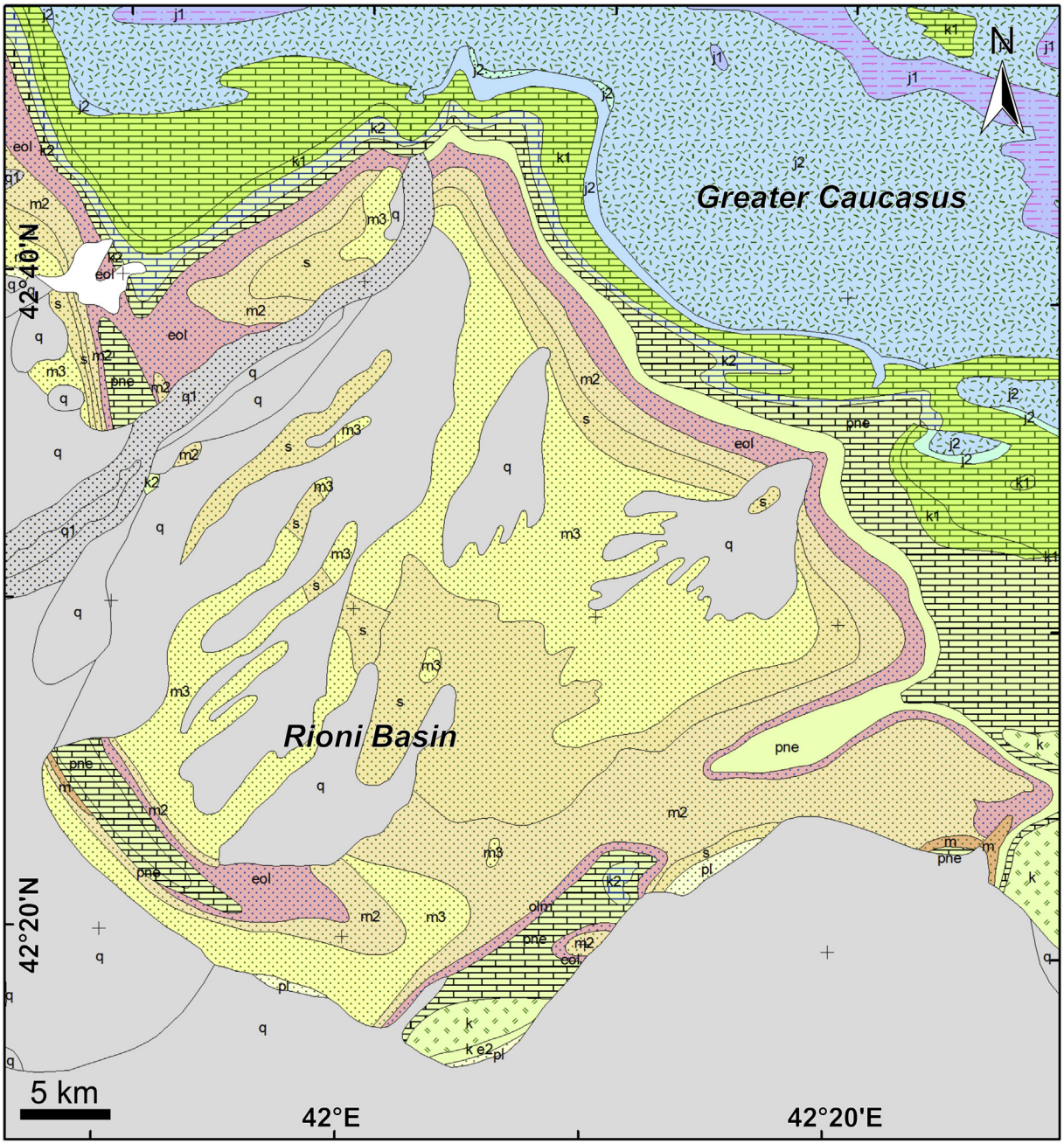

Fig. 2. Geological map of the study area (modified after Adamia and Gujabidze, 2004).

present along the eastern side of the river, suggesting its gradual migration in the opposite direction. The bottom of this series of river beds is interrupted along zone A-B-C (Fig. 6A) by a slightly uplifted, NNW-SSE-elongated topography, standing from a few meters up to 20 m with respect to the valley floor further south. This uplifted zone is transversal to the modern course of the Enguri river, and the latter was forced to deviate towards the SE. Part of the river can still flow southward at point B, but the zone of uplift deflected part of the water course further to the SE, so that the southward flow of the river is possible only at point C.

The above described morphological scarp can be followed more to the south, at the western side of the town of Zugdidi and further south (see the complete trace in Fig. 4). Near Zugdidi, in fact (Fig. 6B), there is a N-S-striking escarpment, facing westwards, about 10–35 m higher than the valley floor further west. This feature can resemble a river terrace escarpment, but detailed measurements of the topography along the foot and the upper edge of the scarp show a slight increase in altitude southwards. If this escarpment was a river terrace, there should have been a slight decrease in altitude in the direction of the river flow, which is to say southwards. However, the observation that the altitude increases in that direction, suggests that the escarpment might represent a tectonic feature, as will be discussed later on. The relatively uplifted area located NE of this escarpment shows evidence of past river migration towards the SE.

Similar evidence is present at several other areas, such as for example in Fig. 7A and B. In these areas there are traces of ancient water courses in the form of abandoned channels or linear sinuous

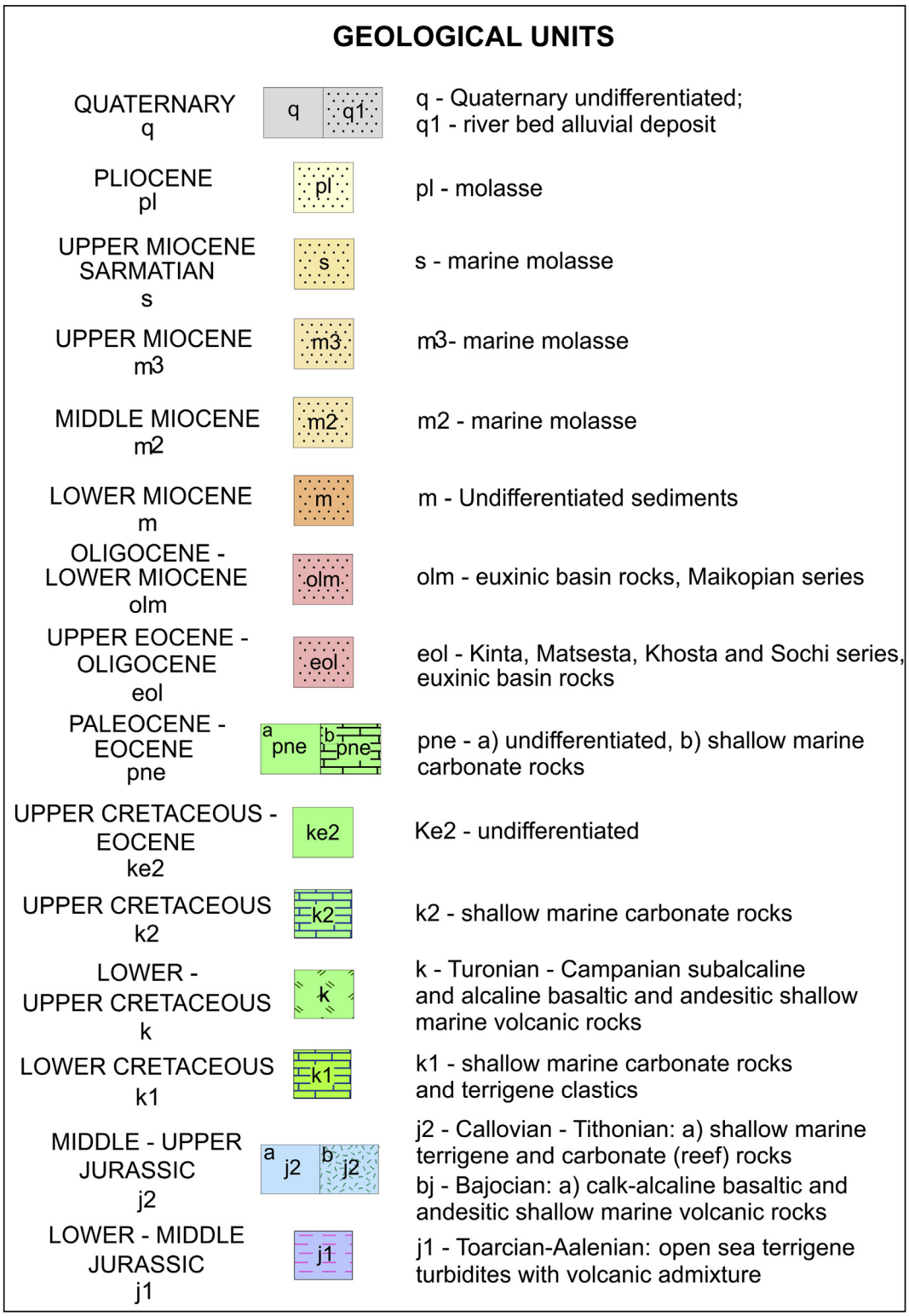

Fig. 3. Lithostratigraphic units in the Rioni basin and their ages (modified after Adamia and Gujabidze, 2004).

zones of very high humidity, visible in infrared satellite images. These ancient water courses are located between topographic highs and the modern river course, indicating past river migration towards the SE. All these areas are located along the frontal part of the uplifted Rioni Basin.

In the northern part of the Rioni Basin uplifted area, at the foothills of the Greater Caucasus, linear features trending WNW-ESE can be observed, which correspond to outcrops of steeply-dipping, substrate carbonatic strata. In the central part of the uplifted area, the morphology is more complex with series of hills with different orientation, corresponding to structural highs linked to folds within the substrate or within Neogene-Quaternary

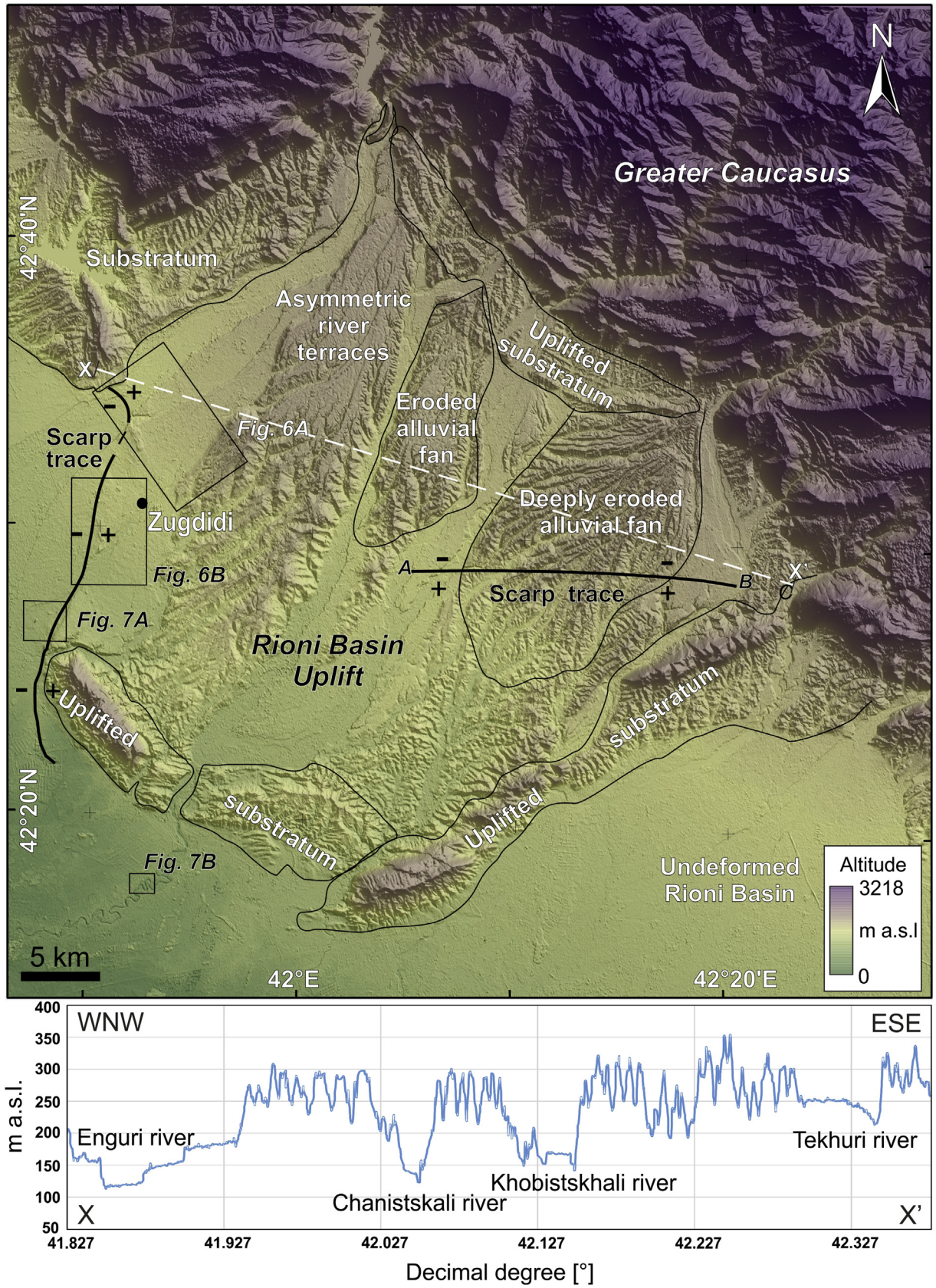

Fig. 4. Digital Elevation Model of the Rioni Basin uplifted area, with indication of the main geomorphological features and location of Figs. 6–7. The graph illustrates the eastward increase in altitude along the trace X-X′.

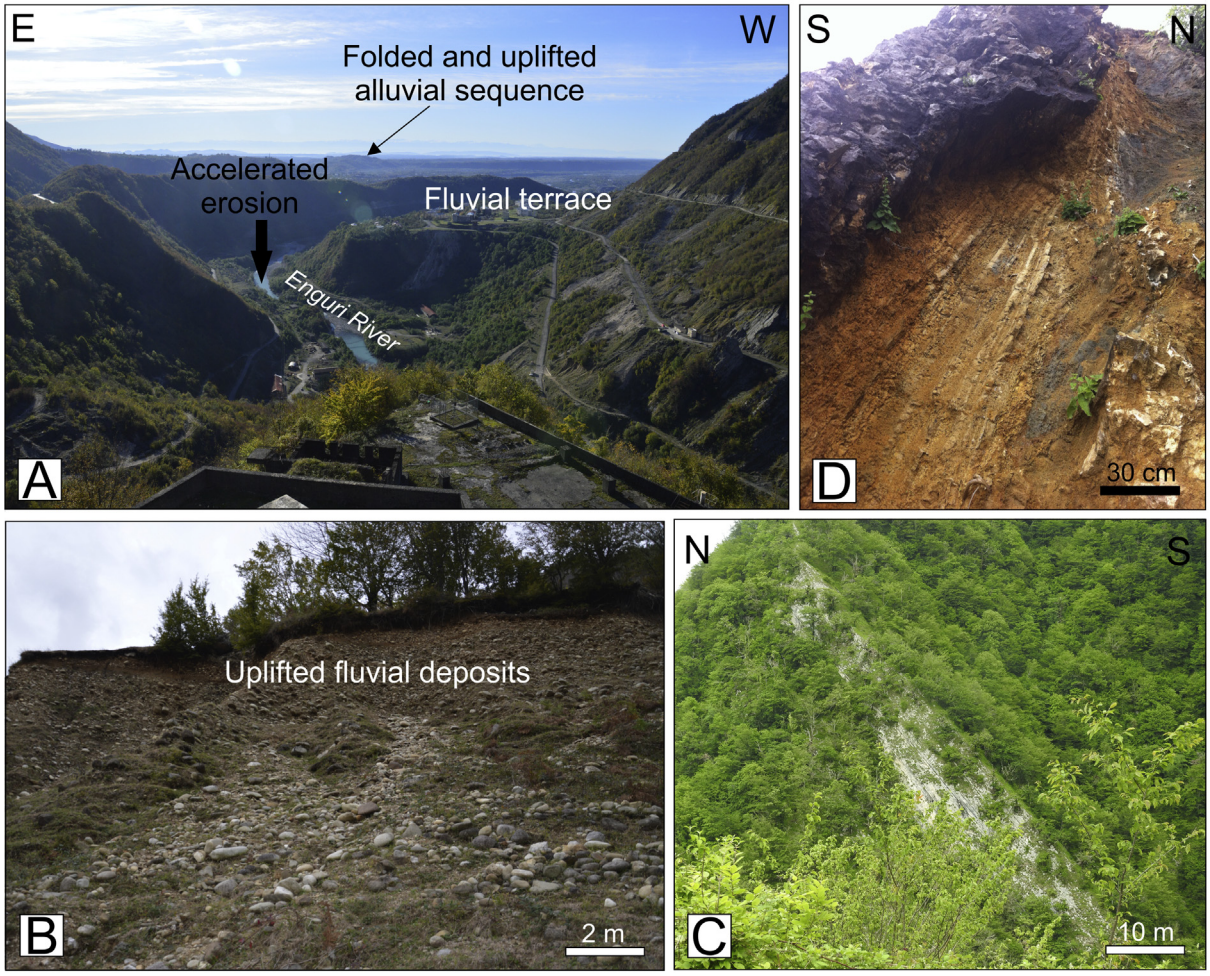

Fig. 5. (A) River terraces and (B) fluvial conglomerates standing 150–200 higher than the present valley floor. (C) Near Enguri, the substrate of carbonatic rocks of the Greater Caucasus shows a dominant dip towards the S, forming a steep monocline. (D) The southern limb of the Senaki fold shows steeply-dipping volcanic and sedimentary strata.

sedimentary deposits, and to old fluvial patterns.

In the central-eastern part of the uplifted area, there is an E-W-striking scarp facing north (points A–B in Fig. 4). The scarp cuts the continuity of all the other landforms and affects the alluvial plane to the east as well (Fig. 8). Along this segment, the Tekhuri river is deflected eastwards (B in Fig. 8) and another river is deflected westwards (from point A to point A′ in Fig. 8). The scarp here is from a few meters high to the east up to 15 m high to the west, as can be noticed from the detailed GPS topographic profiles, which we measured perpendicularly to the scarp (Fig. 9). Further east, the scarp is cut by the Tekhuri river and can be only sparsely observed as far as point C of Fig. 4, where there is a topographic high of the substrate carbonatic rocks. This outcrop, located south of the possible eastward prosecution of the scarp, shows evidence of over-deepening in the form of an about 20-m-deep gorge excavated by the Abasha river. At the western termination of this scarp, the Ochkhomuri river is deflected westwards, whereas a tributary is forced to run parallel to the scarp. The process of river erosion parallel to the scarp may have locally deepened the scarp height, but cannot explain the escarpment formation as a whole. The scarp here, always facing northwards, is as much as 25 m high. The total length of the scarp is 17.5 km along segment A–B, and 22 km if we consider segment A–C (Fig. 4). As can be noticed in Fig. 8, the area south of the scarp (right hand side of the image) is characterized by a slightly upward-convex profile and over-deepened erosive gullies.

3.2. Structural geology

3.2.1. Main structures

Starting from the northern part of the study area, the substrate of carbonatic rocks of the Greater Caucasus shows a dominant dip toward the S and SSW (Fig. 10). The strata dip is around 30–50° and then it increases southwards to 70–90°, forming a monocline (Fig. 5C). Some recumbent folds with gentle interlimb angle are present in correspondence of the monocline, with local over-turning. The general southward steepening of the layers indicates a southern-vergence. No major faults have been observed in the field, whereas fault planes with some cm-long fault striae have been analysed within a secondary tunnel near the Enguri dam, and will be described in the “Microtectonic data” section.

Further south, in the Rioni Basin uplift, substrate carbonatic rocks locally crop out at the foothill of the Greater Caucasus, showing a sub-vertical dip. Further south in the whole central area of the Rioni Basin uplift, there are several scattered outcrops of Neogene-Quaternary terrigeneous deposits. These are mostly represented by claystones, siltstones and sandstones in the lower stratigraphic portions and conglomerates in the upper ones. They are arranged in symmetric folds with interlimb angles from gentle to open. The trend of hinge lines is dominantly N-S to NNE-SSW in the western part and NE-SW to ENE-WSW in the eastern part.

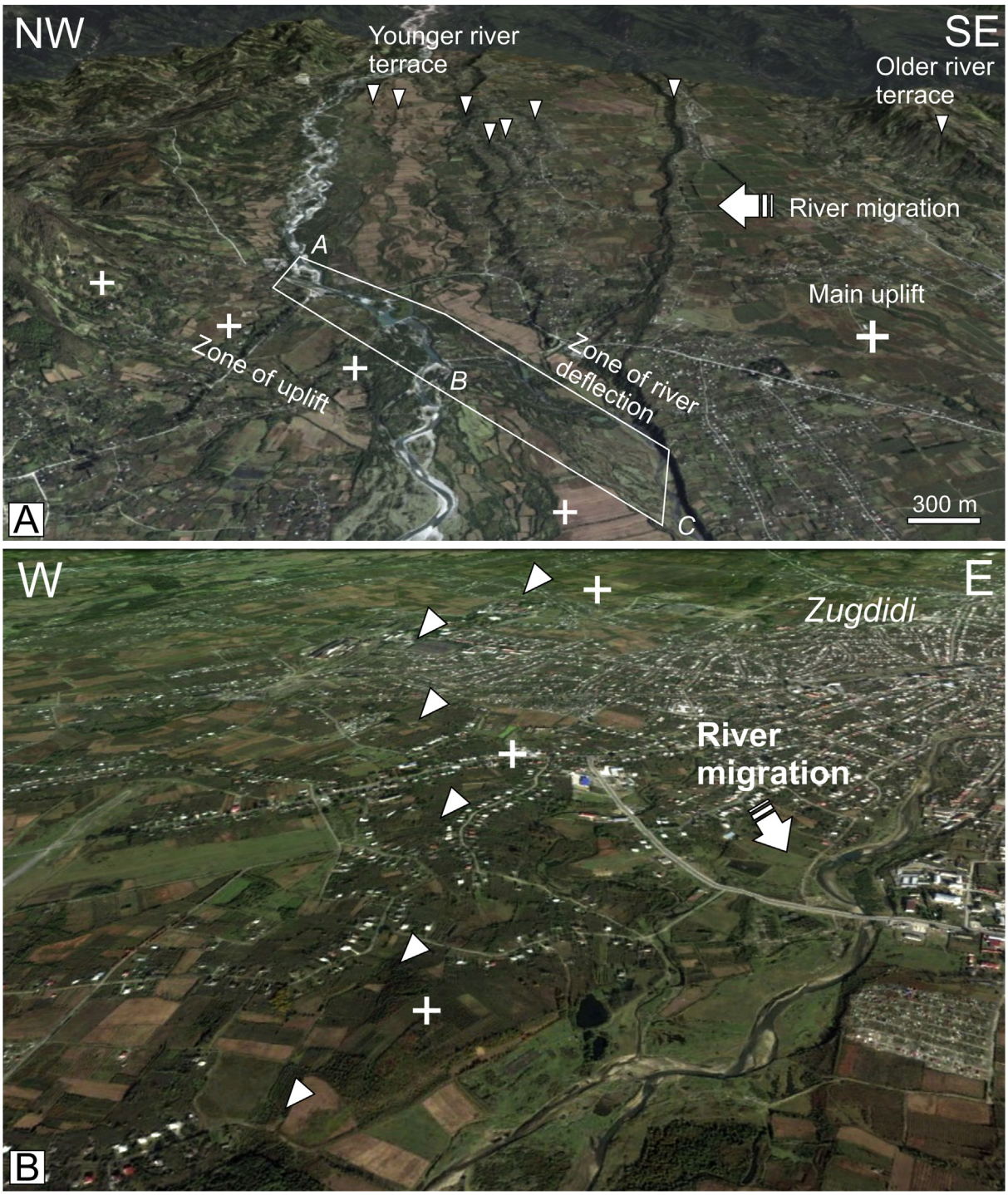

Fig. 6. (A) Westward migration of the northern part of the Enguri River (north of point A) and opposite eastward migration of the southern Enguri segment (south of point B). The white triangles indicate the eight orders of fluvial terraces. The box shows the strip of land along which the Enguri river has been deviated from point A to point B and also to point C. (B) River migration towards SE induced by an elongated zone of uplift; white triangles indicate the possible fault scarp. (GoogleEarth oblique views, 3x vertical exaggeration). Location in Fig. 4.

Along the southern and eastern borders of the uplift area, there is a set of major folds with substrate rocks of carbonatic and volcanic origin cropping out (Figs. 5D and 10). The topographic culminations of the observed folds are higher than the surrounding topography of the Rioni Basin uplift, and the topography flattens out further south and east. The folds will be described in detail in the following chapter.

3.2.2. Fold geometry

One major fold is located in the southwestern part of the Rioni Basin uplift and is known as Tsaishi fold (Fig. 10). This is an anticline with a more complex structure than previously documented, as it is characterized by a sub-vertical dip of the strata to the southwest, locally overturned, and becoming more gentle towards the northeast, where the strata dip 20–40° to the SW. The axial plane dips

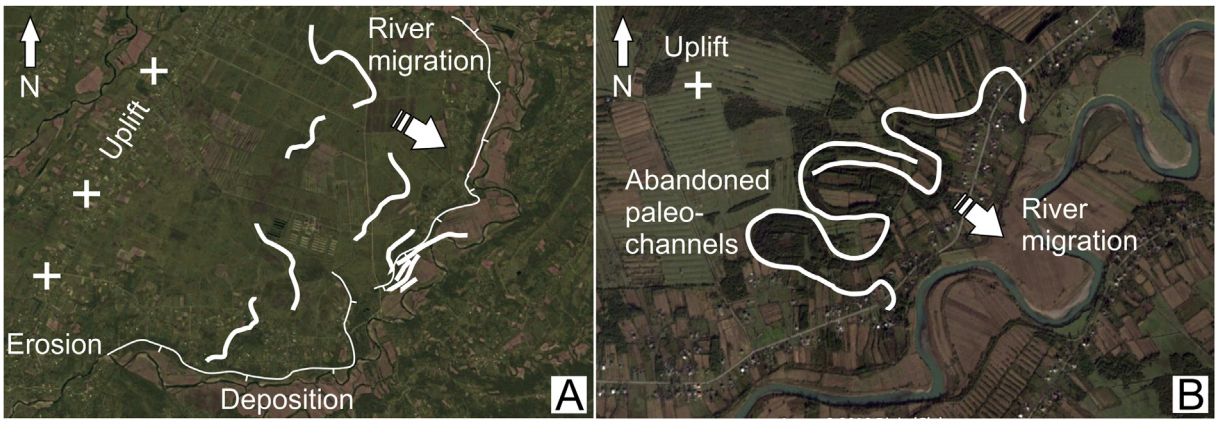

Fig. 7. Migration of rivers induced by differential uplift along the frontal zone of the Rioni Basin uplift. Thick lines represent traces of old river beds as evidenced by differential humidity in infrared satellite images (A) or abandoned channels with still recognizable landforms (B). Thin lines are river terrace escarpments. Crosses indicate zones of uplift. Location n Fig. 4.

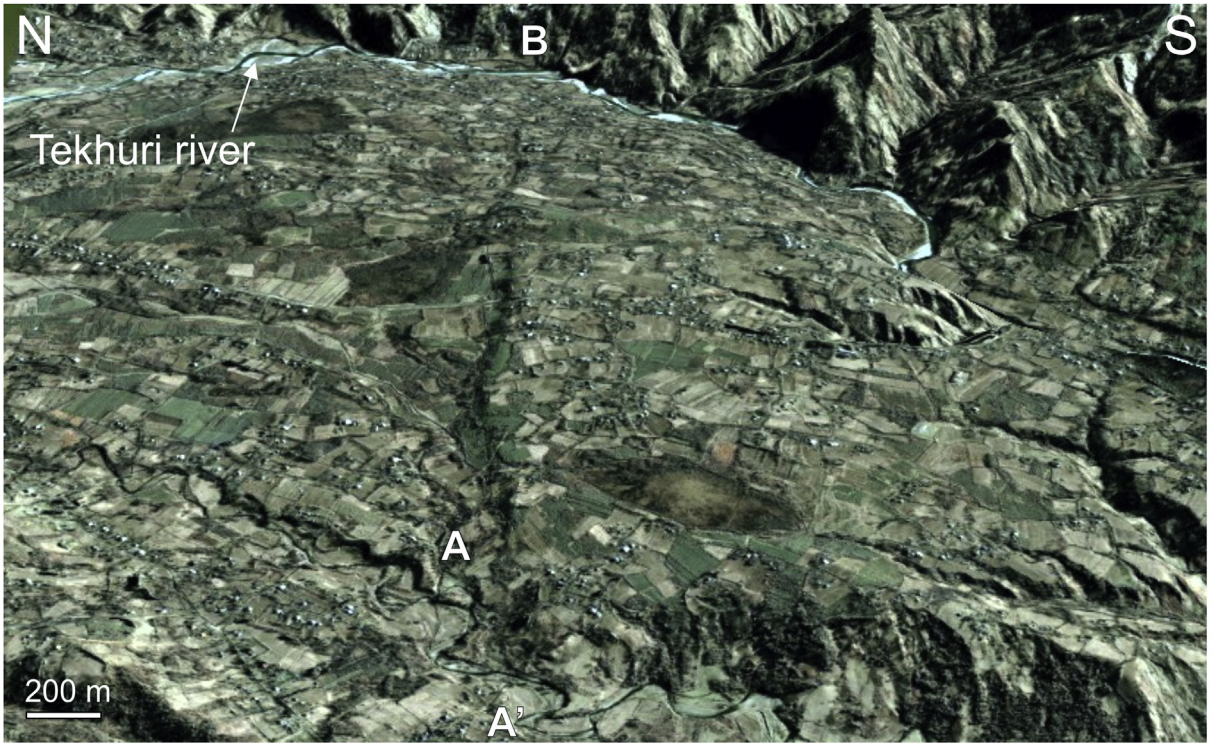

Fig. 8. Oblique view (GoogleEarth, 3x vertical exaggeration) of the eastern part of the E-W scarp affecting the central-eastern area of the Rioni Basin uplift. The scarp here is cut into the alluvial plane of the Tekhuri river. At point B, the Tekhuri river is deflected eastwards, whereas at point A another minor river is deflected westwards at point A′.

about 35° to the NE showing a clear vergence to the SW. The hinge line trends N156° in proximity of the northwestern conical termination of the fold, and N144° along its central and southeastern parts. The fold is 13.2 km long here. Further east, the continuity of strata is interrupted by two narrow valleys trending NNE-SSW, but the dip of the strata allows to recognize the same fold that continues for another 16.2 km. The two valleys should coincide with faults as shown by the possible offset of the fold hinge lines. Here the hinge lines trend, from west to east, N100°, N90°, and N126° near the eastern conical termination. As a whole, this fold in plan view has a sinuous "S" shape and a total length of 29.4 km. It involves rocks of Paleocene to Upper Miocene age, but due to the scarcity of outcrops it has not been possible to observe if younger deposits are folded too.

Further east, separated by a NE-trending lineament, there are another three major folds with hinge lines trending ENE-WSW (Fig. 10). They have an en-échelon left-stepping geometry within a corridor trending N45°. The first fold, located to the SW and here named Senaki, has a N78°-trending hinge line in its western part and a N63°-trending hinge line in its eastern part. The strata dip gently towards the NNW along the northern limb and steeply towards the SSE at the southern limb (e.g. Fig. 5D), with local overturned strata, resulting in a south-vergent anticline (e.g. Fig. 11A). The total length of the outcropping fold is 12.2 km. The fold is affected by some NW-SE-striking right-lateral faults, as in the examples of Fig. 12. Deposits of Cretaceous to Middle Miocene age are involved, whereas younger deposits do not crop out here. The deposits here are made both of sedimentary and volcanic rocks.

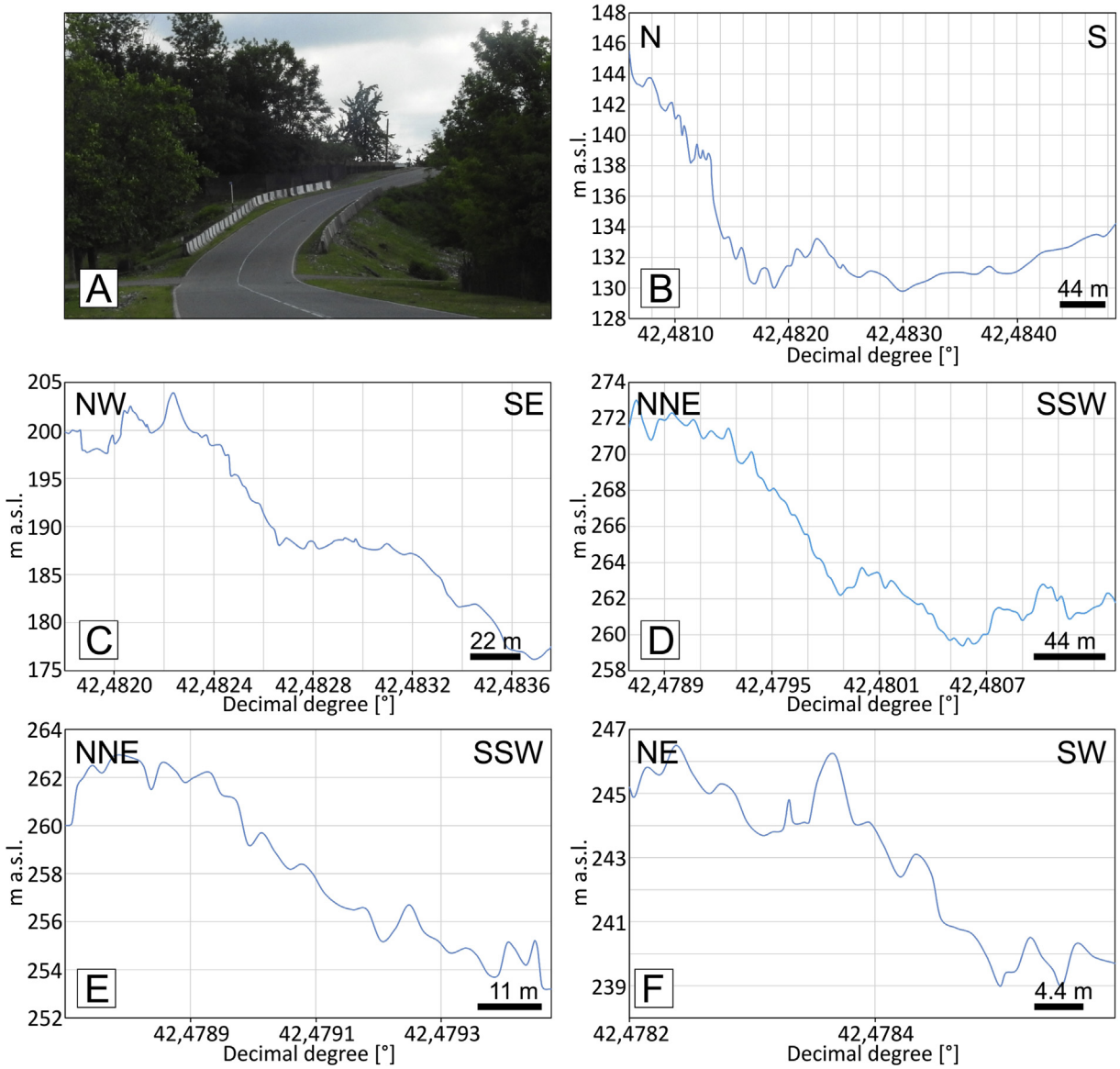

Fig. 9. (A) Photo of the scarp shown in Fig. 8. (B–F) Detailed GPS topographic profiles measured perpendicularly to the scarp. The scarp here is from a few meters high to the east up to 15 m high to the west.

Immediately to the north there is a syncline fold, here named Gakhomela, with a 7.7-km-long hinge line, trending N84°. Further NE, there is another complex major fold, here named Martvili, with a total length of 21.2 km. It has a "S" shape in plan view given by a hinge line trending N67° near its SW termination, N33° in its central part, and N72° towards its NE termination. Strata dip 20–45° to the NW along the northern limb and as steep as sub-vertical along the opposite limb, giving rise to an asymmetric, south-vergent anticline. Deposits of Paleocene to Upper Miocene age are involved, but younger deposits do not crop out here.

Age relationships indicate that all these folds developed after the Upper Miocene, but the scarcity of younger deposits prevents from determining whether these folds are still active, based only on stratigraphy.

In the interiors of the study area, there are folds affecting the Miocene-Pliocene succession and locally also Quaternary deposits (Fig. 10). The folds that affect the Neogene succession have limbs with strata dip in the range 10–30° giving rise to gentle, broad synclines and anticlines. In the western part of the study area, the dip of the strata suggests the presence of folds with hinge lines trending N-S to NNW-SSE. In the eastern part, hinge lines are WSW-ENE to SW-NE. The folds in the interiors of the uplifted area, thus, are parallel to sub-parallel to the folds along its borders. It is worth noting that strata here mostly dip towards the WNW to NW. The same strata attitude has been systematically measured along the E-W scarp of Figs. 8–9, suggesting that the development and geometry of this scarp is independent form any control of strata attitude.

3.2.3. Microtectonic data

Wherever possible, we collected microtectonic data in correspondence of the main structures in the study area (stereograms in Fig. 10). Data comprise slickenside fault planes with kinematic indicators, extensional joints, veins with accretionary fibers, and tectonic stylolites. Special attention was paid to recognizing the order of formation of these structures. Fault planes with tectogliphes have been separated in the field based on their age as resulting from the crosscutting relationships among fault planes of

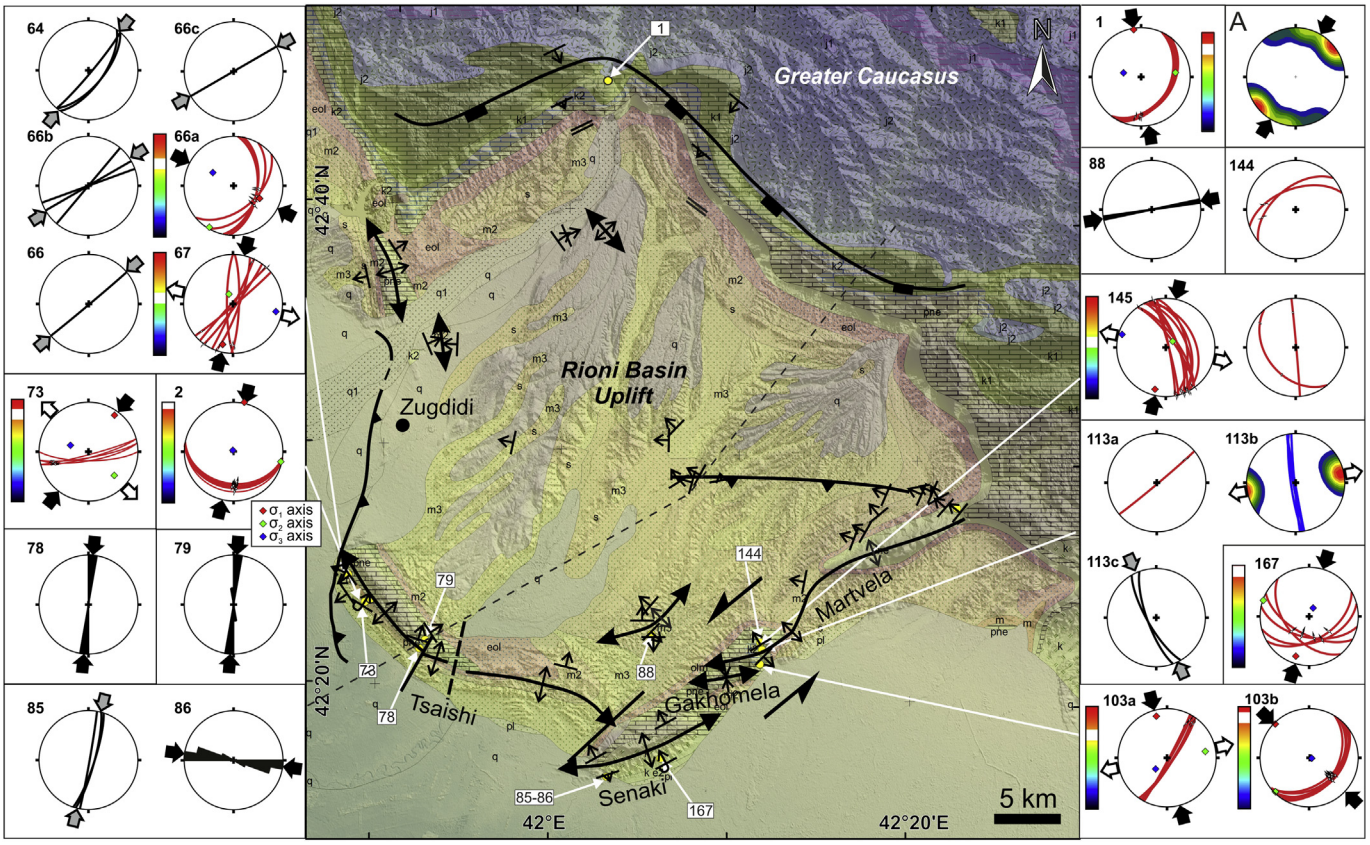

Fig. 10. Map of the structures in the Rioni Basin uplifted area, along with microtectonic data plotted as lower hemisphere Schmidt's stereograms. In these plots, black arrows provide the orientation of σ_1 and white arrows of σ_3 if horizontal, calculated with inversion of fault slip data; the white strip in the color bars indicates the tectonic regime (red = reverse, green = strike-slip and blue = normal). Black arrows provide σ_1 from tectonic stylolites if associated to rose diagrams showing stylolite peaks. Grey arrows provide the σ_{Hmax} derived from extensional joints. Divergent white arrows at site 113b provide σ_3 from crystal fibers. Stereogram "A" in the upper right corner shows the average σ_1 and its dispersion from the younger σ_1 directions surveyed in the whole area. Dashed line shows the trace of the section in Fig. 16. (For interpretation of the references to colour in this figure legend, the reader is referred to the web version of this article.)

different orientation and among faults and lithostratigraphic units. Faults of the same age have been processed with the SG2PS software (Structural Geology to Post Script Converter - http://www.sg2ps.eu; Sasvári and Baharev, 2014), in order to reconstruct the stress tensor. This software allows paleostress inversion using several methods by Turner (1953), Spang (1972), and Angelier (1990). In this work we performed paleostress analyses by using the INVD direct inversion method (Angelier, 1990), because this methodology enables calculating a misfit vector "ν" between the measured and calculated shear vector, and minimizing its length, for at least four different striated faults of the same age.

The results are shown in Table 1 and Fig. 10. Table 1 provides also the plunge and dip of the resulting greatest principal stress (σ_1), intermediate principal stress (σ_2) and least principal stress (σ_3), the ratio (R (Φ)) between the differences of the principal stress eigenvalues, $(\sigma_2-\sigma_3)/(\sigma_1-\sigma_3)$, and the Misfit Angle (Av) expressed as the average angle between computed shear stress and slip vector. The orientation of the σ_1 has been assessed also based on the statistical trend of the peaks of tectonic stylolites, whereas the greatest horizontal principal stress (σ_{Hmax}) has also been determined as orientation of vertical extensional joints. The orientation of the σ_3 has also been measured based on the orientation of the growth of crystal fibres along veins.

In general, reverse faults and strike-slip faults are equally present at most outcrops. Most reverse fault planes dip southwards (e.g. Fig. 11E–F) but the offsets indicate they are minor faults. Nevertheless, it is important to note that shallow brittle deformation here seems to be associated with penetrative faulting in the form of backthrusts with respect to the general southward vergence. Transcurrent faults are mostly given by right-lateral strike-slip displacements along vertical planes striking NW-SE to N-S (e.g. Fig. 12A–B). Vertical left-lateral strike-slip faults are also present with dominant NNE-SSW to NE-SW strikes.

In Fig. 10, the microtectonic observations are differentiated in terms of data typology. The most represented directions of the σ_{Hmax} are in the range N5-40° with the average value at N30° (stereogram A in Fig. 10) as obtained by fault slip data inversion, crystal fibre growth, tectonic stylolites, and extensional joints. Fault slip data and stylolites are consistent with $\sigma_{Hmax} = \sigma_1$. Where more than one deformation phase has been recorded by structures, it resulted in σ_{Hmax} orientation varying apparently with time. As an example, at the northwestern part of the Tsaishi fold, the older structures are represented by reverse faults (e.g. Fig. 11E). The oldest age can be attributed based on the observation that all the other structures interrupt the continuity of these reverse faults here, and also by the reverse fault dip angles up to 50° suggesting possible tilting. The reverse faults give a subhorizontal N110° σ_1 (site 66a, Fig. 10). Younger strike-slip faults give a horizontal N20° σ_1 (site 67), followed by the youngest structures, here represented by open fissures that suggest a N40-50° σ_{Hmax} (sites 64, 66b and 66). These data indicate an apparent gradual clockwise rotation of σ_{Hmax} with time. At the central part of the Tsaishi fold, a series of striated backthrusts results in a N10° σ_1 (site 2), consistent with the direction of N5° of the σ_1 based on stylolites a few km to the

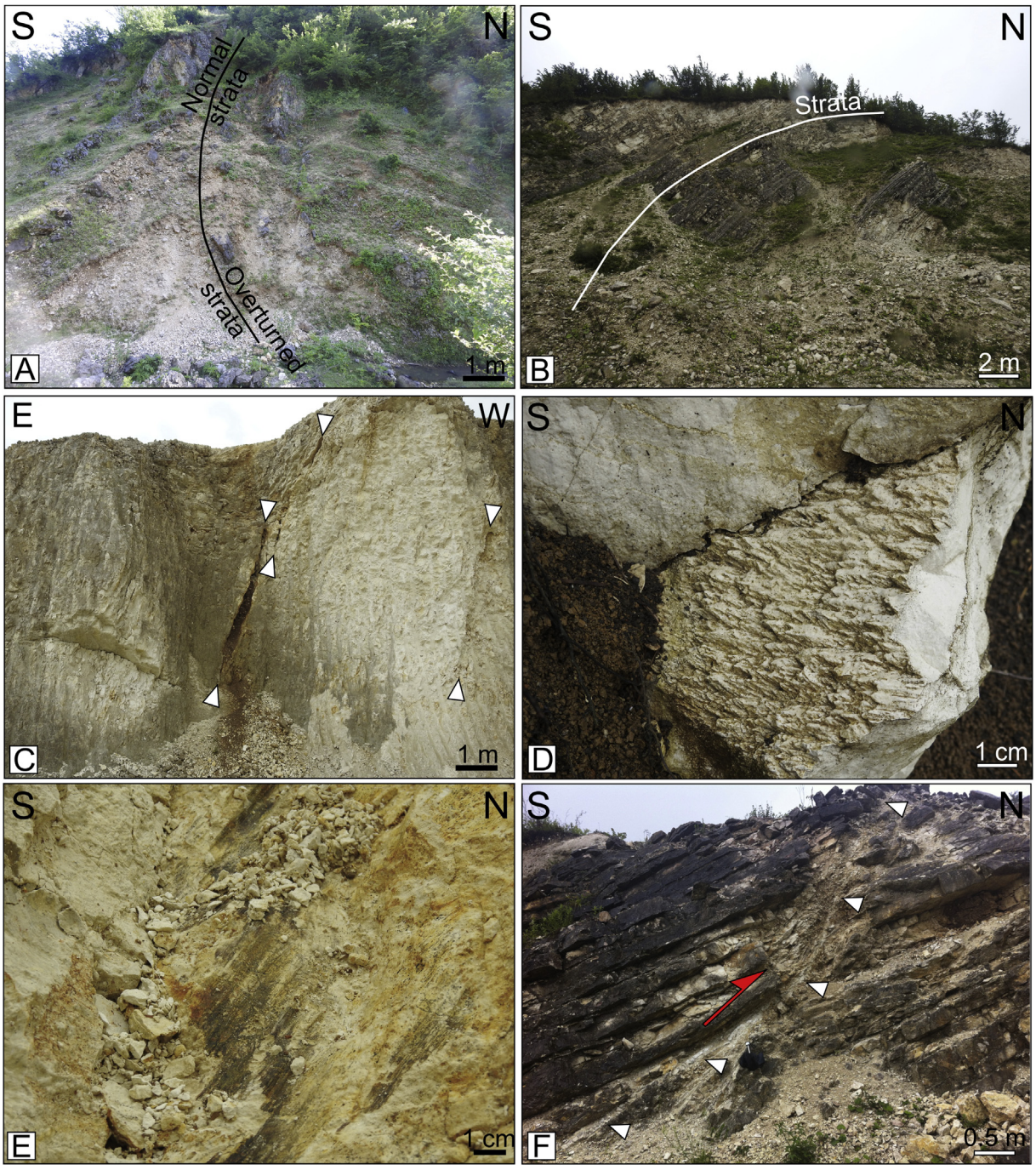

Fig. 11. (A) Overturning of the strata at the southern limb of the Senaki fold. (B) Steepening of the strata at the southern limb of the Tsaishi fold. (C) Example of the youngest structures at the Tsaishi fold given by N-S-striking extensional fractures. (D) Stylolites suggesting N-S compression at the Tsaishi fold. (E) Example of striated reverse fault at the southern limb of the Tsaishi fold. (F) Example of back-thrust here represented by a south-dipping reverse slip plane, observed in the central part of the Tsaishi fold.

southeast (sites78-79).

Near the western termination of the Senaki fold, the older structures are represented by stylolites indicating a N105° σ_1 (site 86), followed by the development of vertical extensional joints that give a N14° σ_{Hmax} (site 85). These data indicate a possible major apparent clockwise rotation of σ_{Hmax} with time. At the central part of the Senaki fold, reverse faults dipping SSW (site 167) give a N18° σ_1.

At the southern flank of the southwestern part of the Martvela anticline, the older structures are represented by reverse faults dipping to the southeast (site 103b) that give a horizontal N135° σ_1. These structures have been followed by the development of NE-SW left-lateral transcurrent faults that give a N169° σ_1 (site 103a), thus resulting again in an apparent clockwise rotation over time. At the northern flank of the same fold, NNW-SSE right-lateral strike-slip faults resulted from a N14° σ_1 (site 145), and crystal fibres give a N85° σ_3 that corresponds to a N175° σ_{Hmax} (site 113b). The age relationships between the latter two sites are not clear. The youngest structures here are extensional joints that give a N160° σ_{Hmax} (site 113c).

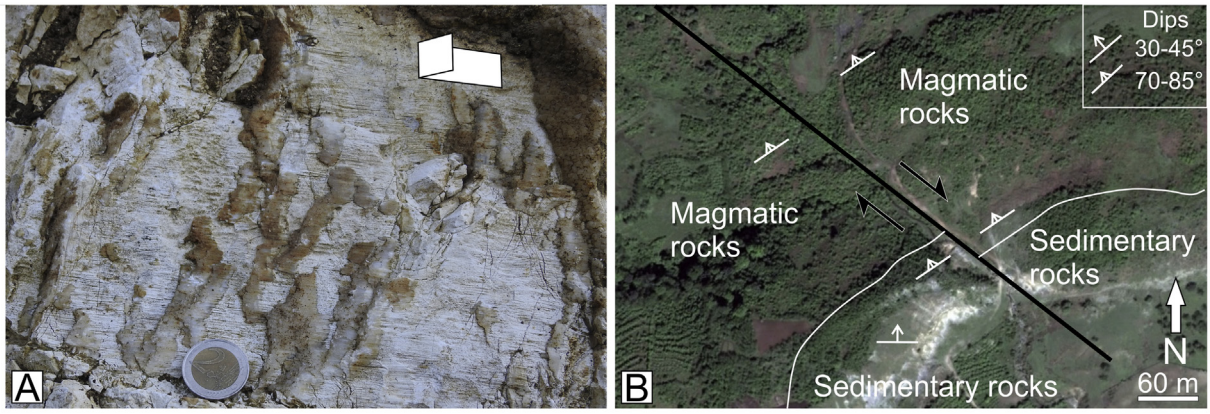

Fig. 12. (A) Example of right-lateral strike-slip fault in carbonatic rocks with accretionary fibers at the Senaki fold. (B) Example of NW-striking right-lateral fault affecting the Senaki fold, with offset of the sub-vertical limit between Cretaceous magmatic and sedimentary rocks.

Table 1
Results for paleostress calculation.

Site	Lat (dd°)	Lon (dd°)	N. of data	σ1 (plg/dip)	σ2 (plg/dip)	σ3 (plg/dip)	R (ϕ)	Av Misfit Angle	Tectonic regime
2	42.392	41.827	6	013/00	103/00	207/90	0.483	2.5	PURE COMPRESSIVE
66a	42.409	41.804	5	118/39	209/01	300/51	0.094	5.7	TRANSPRESSIVE
67	42.408	41.805	7	193/13	338/74	101/09	0.322	13.3	PURE STRIKE SLIP
73	42.390	41.822	6	43/17	141/25	283/59	0.645	2.1	PURE COMPRESSIVE
1	42.757	42.0340	6	352/07	085/29	250/60	0.519	1.4	PURE COMPRESSIVE
145	42.371	42.192	10	193/11	058/75	285/10	0.337	3.5	PURE STRIKE SLIP
167	42,289	42.102	6	197/13	288/04	033/76	0.874	4.6	RADIAL COMPRESSIVE
103a	42.356	42.193	5	346/17	083/21	221/63	0.169	2.1	TRANSPRESSIVE
103b	42.356	42.193	7	314/05	224/01	125/85	0.741	1.7	PURE COMPRESSIVE

In table are reported: site number and location (Lat and Lon); number of data used during the inversion process; plunge and dip of resulting σ_1, σ_2 and σ_3; ratio (R (Φ)) between the differences of the principal stress eigenvalues, (σ2−σ3)/(σ1−σ3); Av Misfit Angle = average angle between computed shear stress and slip vector; resulting tectonic regime.

Finally, in the northernmost part of the study area in an artificial tunnel near the Enguri dam (site 1), several fault planes show oblique slickenside lineations that give a N175° σ_1.

3.3. Seismicity

The seismicity is shown in Fig. 13, which provides data from both the historical (before 1900 AD) and instrumental catalogue. The Intensity of historical earthquakes ranges up to 9 (MSK scale) (Varazanashvili et al., 2011). The M_W of instrumental events is in the 2 to 5.3 range.

The strongest seismic events in the investigated area during the instrumental period are: Samegrelo-Svaneti, 1930 (M_W = 5.3); Menji, 1941 (M_W = 5.2); Western Georgia, 1948 (M_W = 5.0); Gegechkori, 1957 (M_W = 5.3); Achigvari, 1958 (M_W = 5.2); Rechkhi, 1979 (M_W = 5.0). It should be stressed that the epicenters are mostly located along the northwestern and southeastern sides of the uplifted area. In the southeastern part, a cluster of earthquakes with a NE-SW trend can be recognized; this cluster coincides with the zone of en-échelon folds previously described. The cluster along the northwestern part of the uplifted area is represented by the epicenters of the December, 1979 Rechkhi earthquake swarm, made of foreshocks, aftershocks and two main events of M_W4.9 and 5.0. The earthquake depths were between 2 and 5 km. These earthquakes occurred in the area of Gali water reservoir (belonging to the Enguri hydroelectrical scheme) in coincidence with the filling of this reservoir and of Enguri reservoir. It is important to note that the distance between these reservoirs and the earthquakes was at minimum of 19 km, and the seismic activity of this area is still ongoing. For example, in July, 2010 an earthquake with M_W = 4.9 occurred in the same area. It is thus highly questionable that this swarm was originated by reservoir infilling. In fact, high seismicity linked to tectonic stresses is often manifested (approximately 20 yr period) as earthquake swarms in the area. For example, in June–July, 1941, there were earthquakes swarms with main shocks of M_W = 5.0, M_W = 5.0 and M_W = 5.2). In January, 1957 there was also the large Gegechkori earthquake swarm, which comprised three main shocks of M_W = 5.2, M_W = 5.2 and M_W = 5.3) and several foreshocks and aftershocks.

Instrumental earthquake depths for the study area are provided in the histogram of Fig. 13, showing the number of earthquakes with $M_W \geq 4.4$ vs. their depth for the period 1900–2014. The graph shows also the trend line that was calculated through the moving averaging by step 2. In this map we plotted only those events which have a reliable depth estimation taken from the new Georgian catalogue. Most hypocenters are located at depths from 2 to 19 km, and most have originated at depth of 9–10 km.

It is key to underscore that one main historical earthquake (M_W = 6.1, Io = 8–9, MSK) did occur immediately southwest of the Tsaishi anticline (Fig. 13). This seismic event took place in 1614 AD (Tsaishi earthquake, Varazanashvili et al., 2011). This epicenter is located exactly along the trace of the previously described escarpment (Figs. 4 and 10A).

Some new fault plane solutions for instrumental earthquakes were calculated for the study area (Fig. 13). In order to perform the identification of the fault planes we used the first motion polarity technique. Only earthquakes for which the number of polarities is equal or more than 8, and azimuthal gaps were less than 180, were selected. All the focal mechanism solutions have a reverse kinematics. The slip fault planes strike NE-SW for five solutions and

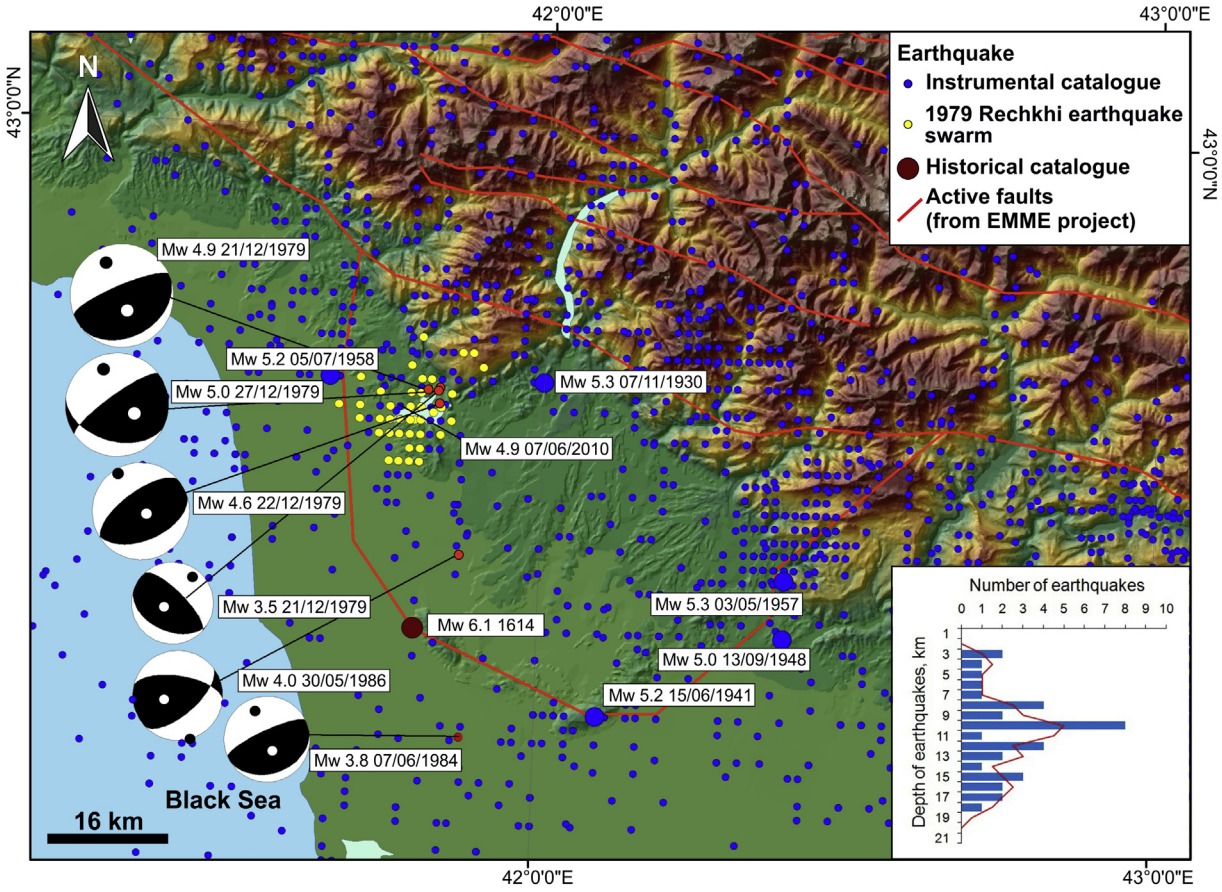

Fig. 13. Distribution of instrumental (yellow and blue circles) and the main historical (brown circle) epicentres in the study area. Earthquake focal mechanism solutions have been computed in the framework of the present work. The histogram shows the number of earthquakes with $M_W \geq 4.4$ vs. their depth for the period 1900–2014 in the study area, together with trend line. (For interpretation of the references to colour in this figure legend, the reader is referred to the web version of this article.)

NW-SE in one case. Following the classification scheme of World Stress Map (Zoback, 1992; Heidbach, 2009) the stress regime here corresponds to TF (thrust fault).

3.4. Seismic sections

A series of unpublished seismic reflection sections have been interpreted here in order to integrate the data gathered in the field with geophysical evidence of deeper structures (Figs. 14 and 15). We obtained three, NE-SW trending (A–B, C–D, E–F) and one, NW-SE trending (G-H) seismic reflection sections. These are concentrated in the southwestern part of the study area, around the Tsaishi fold. Identification of stratigraphic units at depth was based on outcrop correlations and two deep wells data (box in Fig. 14C). Sections A–B, C–D and E–F reveal, in their uppermost sections, the presence of the south-vergent Tsaishi anticline, south-vergent thrust faults (F1, F2, F3, F4, F5) and north-vergent back-thrusts (BT1, BT2, BT3).

The Tsaishi anticline is a fault-propagation fold whose front limb is broken by thrust faults. The lower part of the sections is marked by the upper detachment, which correlates with the Upper Jurassic evaporites. Above there are units represented by Tertiary, Cretaceous and Upper Jurassic strata. The south-vergent thrust faults, backthrusts, and reactivated and non-reactivated extensional faults in the top section, are the clearest faults observed from the time-migrated seismic data. The middle section between the upper detachment and lower detachment is characterized by blind wedging of the thrust sheets. The bottom section below the lower detachment zone is autochthonous. In the underlying duplex, the thrusts flatten upward into the detachment zone, forming the wedge-shaped triangle zone geometry (Fig. 14B and D). South-vergent duplexes involve Middle-Lower Jurassic strata. All the seismic sections suggest that the Rioni Basin tectonics is of the thin-skinned type.

4. Discussion

4.1. Geometry of main structures

The study area is limited to the north by a wide asymmetric fold with gentle-dipping limb strata to the north, and steep-dipping strata to the south, which are locally verticalized. This structure is morphologically represented by the southern front of the Greater Caucasus, where the average altitude drops from 1500 to 2000 m a.s.l. to the 200–300 m a.s.l. of the Rioni Basin. Our field investigations has not enabled recognizing main outcropping active faults along this part of the Caucasus front. Although we acknowledge that the area is heavily covered by forests and of difficult access, the outcrops here do not show any major fault. The only evidence of faulting has been observed inside the artificial tunnel near the Enguri dam. Here, microtectonic observations indicate the presence of left-lateral oblique faults dipping N120° (site 1 in Fig. 10). Our field data collected at the Enguri dam zone suggest that this structure is the effect of fault-propagation folding (A in Fig. 16). A distinctive marker of fault-propagation folds, in fact, is the asymmetric fold profile characterized by a steeply dipping to

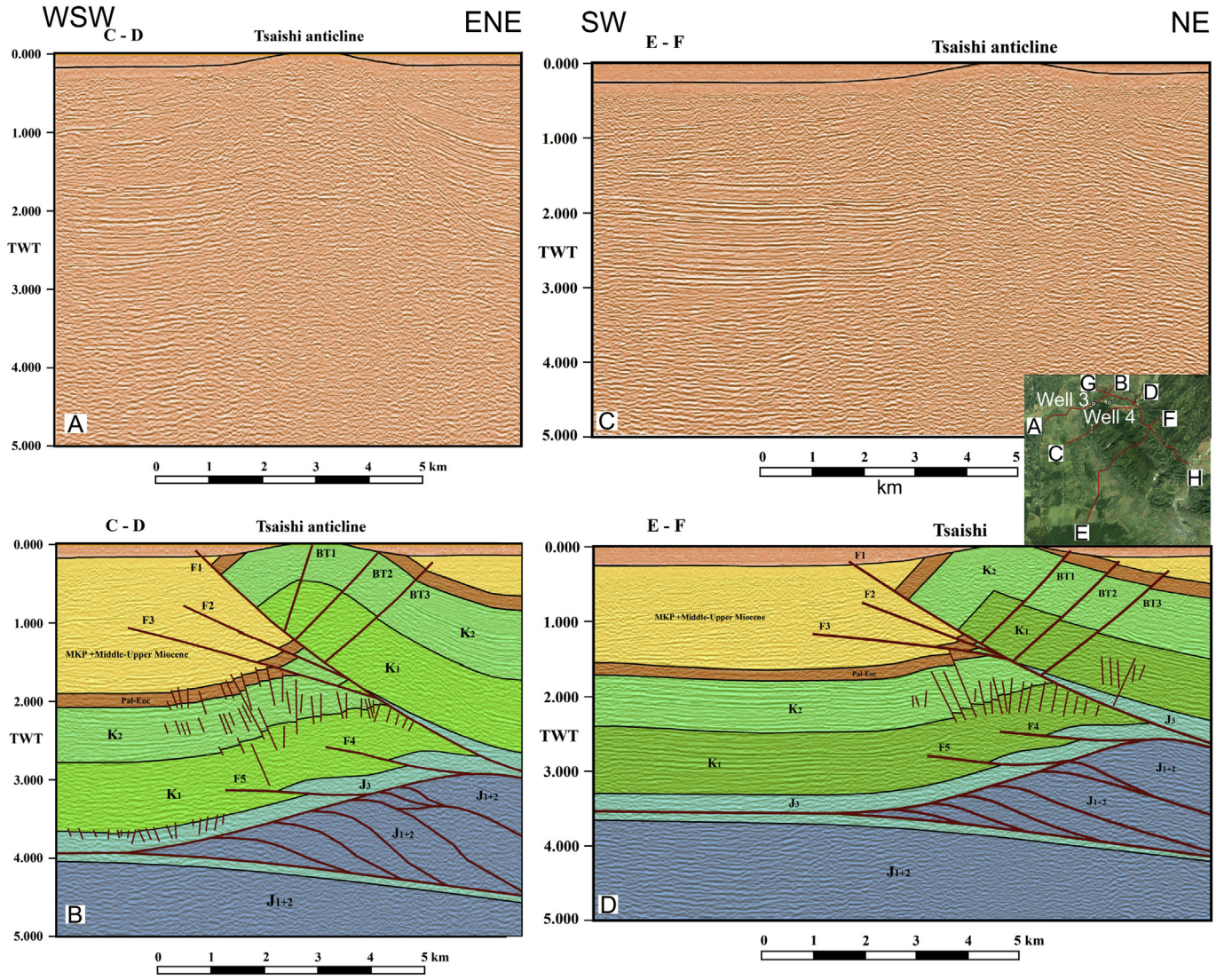

Fig. 14. (A) Uninterpreted and (B) interpreted seismic reflection profiles C–D, and (C) uninterpreted and (D) interpreted seismic reflection profiles E–F. Location in box. Abbreviations: J1+2 Lower and Middle Jurassic; J3 Upper Jurassic; K1 Lower Cretaceous; K2 Upper Cretaceous; Pal-Eoc Paleocene-Eocene; MKP Maikopian (Oligocene-Lower Miocene).

overturned forelimb and a gently-dipping back-limb. Fault slip progressively decreases along the low-angle propagating ramp, terminating upsection in a blind tip with shortening accomplished by folding (Williams and Chapman, 1983; Suppe and Medwedeff, 1990; Mitra, 1990). This model is consistent with the verticalized strata observed in the field at the forelimb.

On the contrary, fault-bend folds are formed by the passive accommodation of hanging-wall strata over a thrust fault whose dip changes (B in Fig. 16) (Suppe, 1983; McClay, 2011). The distinctive geometry of a fault-bend fold is the more symmetric hanging-wall fold profile characterized by a broad anticline with gently-dipping forelimb and back-limb.

Combining the field data with our seismic sections and those published in Banks et al. (1997), we have reconstructed the structural crustal section of Fig. 16. In the northern part of this section, outcropping strata are arranged into the asymmetric south-vergent fold, interpreted as a fault-propagation fold; this is consistent with a shallow reverse fault interpreted by seismic sections. At a deeper level, the seismic data of Banks et al. (1997) indicate the presence of a thrust plane below the southern frontal zone of the Greater Caucasus. The fault gently dips northwards and is here located at a depth of 5–9 km. The geometry of this deeper part of the frontal structure should correspond to a leading anticline-syncline pair, originated as a fault-bend fold with the main ramp located further north. The involved rocks here are represented by Jurassic deposits and Paleozoic units.

Further south, the tectonic block located above the footwall flat is marked by the presence of deposits of Cretaceous and Tertiary age. These are slightly deformed, in agreement with the field data, where gentle folds are present in the interior of the Rioni Basin uplift. Based on our field data, this tectonic block is affected by a southward-dipping backthrust (Fig. 16). This fault is expressed at the surface by the E-W-striking scarp that offsets Quaternary deposits, illustrated in Fig. 8. As also shown in Fig. 10, along this scarp the strata dip toward the WNW and hence we can rule out a morphoselection origin. We also have to rule out that this scarp is the expression of a river terrace, because rivers here have always been flowing perpendicularly to the scarp strike. The rocks that crop out at the footwall block are represented by silty and clay deposits of probable Upper Miocene age. The deviation of the rivers, the over-deepening of the hanging wall block surface, the fact that the fault scarp is cut into Miocene-Quaternary deposits,

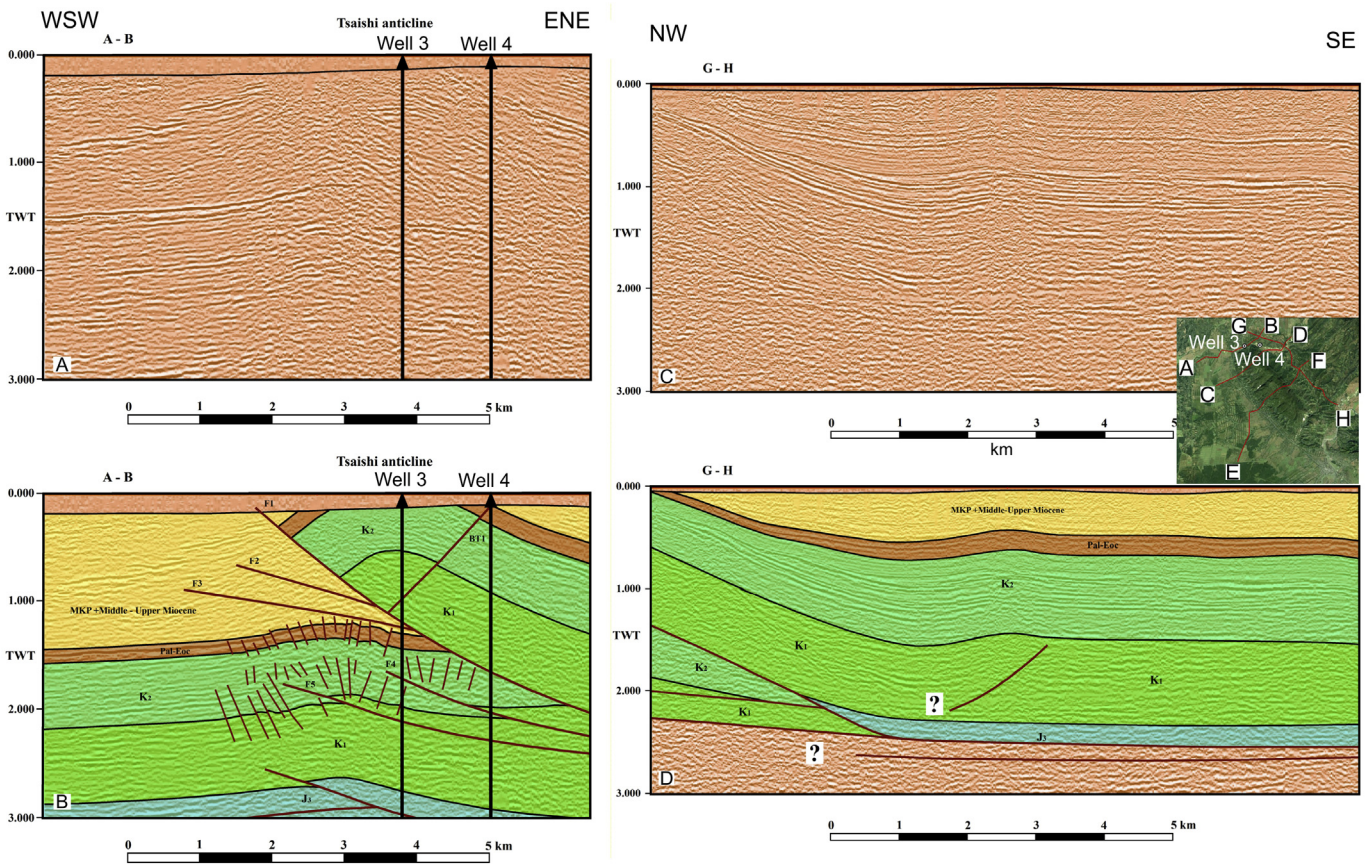

Fig. 15. (A) Uninterpreted and (B) interpreted seismic reflection profiles A–B, and(C) uninterpreted and (D) interpreted seismic reflection profiles G–H. Location in box. Abbreviations: J1+2 Lower and Middle Jurassic; J3 Upper Jurassic; K1 Lower Cretaceous; K2 Upper Cretaceous; Pal-Eoc Paleocene-Eocene; MKP Maikopian (Oligocene-Lower Miocene).

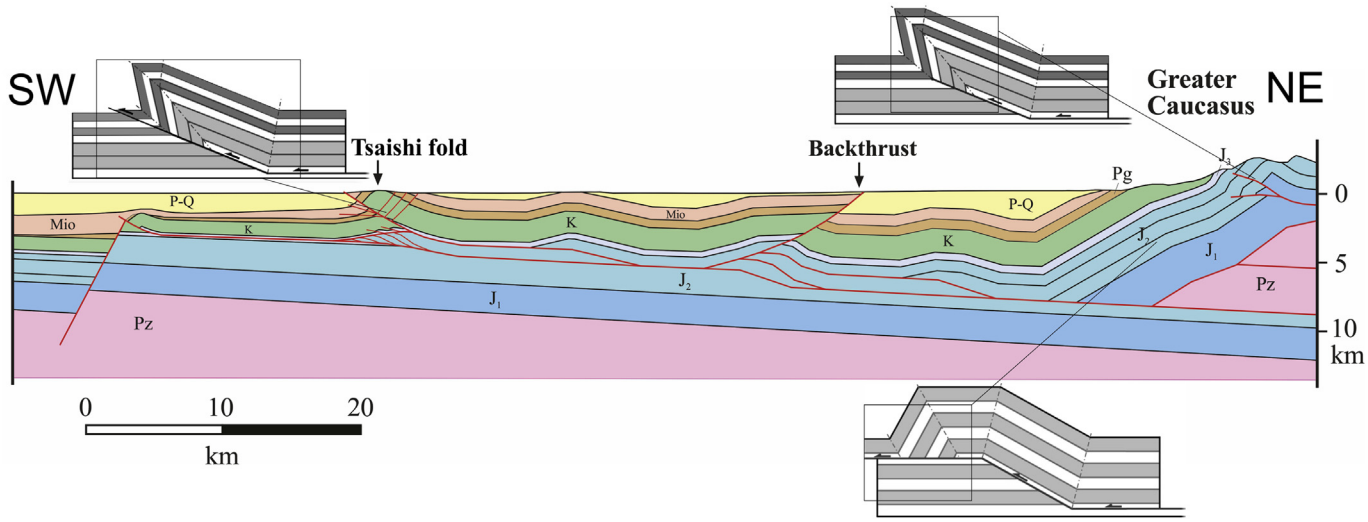

Fig. 16. Structural crustal section obtained by combining our field data and seismic reflection sections with data published in Banks et al. (1997). Pz Paleozoic, lJ lower Jurassic, mJ middle Jurassic, uJ upper Jurassic, lK lower Cretaceous, uK upper Cretaceous, Pg Paleogene, Sar Sarmatian, P-Q Pliocene-Quaternary. Schematic geometric model of (A) a fault-propagation fold (modified after Suppe and Medwedeff, 1990), and (B) a fault-bend fold (modified after Suppe, 1983). The fault-bend fold is characterized by a relative symmetry between the forelimb and backlimb, whereas the fault-propagation fold has steep to overturned strata in the forelimb. (C) Shows a fault-propagation fold with the thrust reaching the surface. Section trace in Fig. 10.

and the presence of earthquake shallow hypocenters south of the scarp, indicate that this is a recent, probably active, back-thrust.

Further south, based on seismic data, the tectonic block above the footwall flat is affected by a north-dipping splay fault. This is a blind fault connected with a shallow fault-propagation fold. More to the south, our seismic sections show the presence of another splay fault departing from the main thrust, forming a north dipping ramp that terminates immediately southwest of the Tsaishi fold.

Our field data indicate that this is an asymmetric fold with steep-dipping forelimb strata and more gentle-dipping back-limb strata. Moreover, the morphological scarp observed west of the town of Zugdidi and immediately southwest of this fold, might represent the emersion of the thrust splay fault. This interpretation is consistent with the aligned morphological scarps facing towards the west (illustrated in Fig. 4), with the migration of rivers on the hanging-wall block as a response to uplift, and to the occurrence of the 1614 Tsaishi earthquake exactly along this structure. This scarp cannot be related to a river terrace, in that it has a different orientation with respect to the rivers and the average altitude increases down-valley along the scarp edge. All these data suggest that the Tsaishi fold is a fault-propagation fold with the thrust plane propagated through the entire fold rock succession, under the western segment of the fold (C in Fig. 16). Underneath the eastern segment of the Tsaishi fold instead, the thrust tip is still hidden. Below the Tsaishi fold, a local tectonic wedge has been developing. Finally, further south, the seismic sections indicate the presence of another blind thrust. As a whole, tectonic units are arranged into an imbricate series of south-vergent thrust slices.

4.2. Tectonic evolution

The Rioni Basin has been the site of marine sedimentation during Tertiary times, followed by the emplacement of continental deposits during the Upper Miocene-Pliocene. These rocks represent a molasse-type deposition in an E-W-elongated depression limited to the north and south by the growing Caucasus mountain belts. The presence of past extensional tectonics is demonstrated by the normal faults found in the seismic sections. These faults are limited to the lower part of the sections since they displace deposits of Jurassic to Paleogene age. The normal faults do not cross deposits of Sarmatian age and younger. The deposits of the geological time interval Paleogene–Middle Miocene are condensed to absent beneath the Rioni Basin, reflecting non-deposition and erosion during foreland basin development (Robinson et al., 1996; Banks et al., 1997). Therefore, the main filling of the Rioni foreland basin took place in Late Miocene to Quaternary times.

All deposits are involved in reverse faults and folds, indicating that inversion tectonics occurred here since the Sarmatian. Compressional tectonics took place through the development of main, north-dipping ramp-and-flat structures, with flat surfaces mostly developed along a detachment level represented by upper Jurassic evaporites (Banks et al., 1997). The folds started to grow as they moved along the ramp-and flat structures, accompanied by the development of minor reverse faults, most of which dipping southward. Thus, penetrative minor deformation took place in the form of back-thrusting. This was followed by the formation of minor transcurrent faults, and locally strike-slip tectonics nucleated along a few major structures. This is suggested by the presence of the NNE to NE-trending lineaments that offset the frontal folds. Although it has not been possible to directly observe these fault planes, their rectilinear trace in plan view and the presence of several strike-slip minor faults with the same geometry, are consistent with this interpretation. These major transcurrent faults also acted as nuclei for river erosion, enabling deepening of a few major river beds across the folds. The latest brittle deformations occurred in the form of vertical extensional joints in the shallowest part of the rock succession, whereas at deeper levels, the main north-dipping thrust propagated towards the surface in the western part of the study area, and a main back-thrust developed in the eastern interior of the uplifting area and reached the surface.

The youngest directions of the σ_{Hmax} are quite homogeneous all over the area following a dominant N-S to NNE-SSW trend. This corresponds to σ_1, consistent also with GPS data (Reilinger et al., 1997, 2006; McClusky et al., 2000) and with focal mechanism solutions at the regional level (Tsereteli et al., 2016). Paleostresses, on the other, hand, are much more complex and show different orientations over time. We suggest that these different orientations do not correspond to changes in the principal stress direction over time, but they are the effect of rotation of the folds (or at least of some portions) under a simple shear regime, similarly to what was found for example during the development of en-échelon folds in the Algerian Atlas (Ferrari et al., 1990). Our preliminary field data at Rioni Basin uplift suggest a dominant anti-clockwise sense of rotation of the structures. Although this rotation is consistent with the en-échelon left-stepping geometry of the folds within a left-lateral shear zone, we believe that the existing data are still not sufficient for reaching a definitive conclusion on the sense of transcurrent motions or other processes that can be associated with the rotation of these folds; therefore, to accomplish the above goal, more field investigations are necessary.

The contraction and uplift amounts are differential with a gradual increase eastward. This is shown by a series of clues: 1) the average altitude increases eastward as illustrated in the graph of Figs. 4 and 2) the valley bottom altitudes increase in the same direction, 3) in general, the main rivers migrated westward as indicated by the asymmetric several orders of river terraces present on the eastern sides of the valleys, 4) the Upper Miocene-Quaternary succession in the interiors of the uplifted area mostly dips towards the WNW as resulting from differential uplift, 5) folds are more developed in the eastern side of the study area, and 6) a major back-thrust developed in the eastern part of the area in response to larger contraction here. This differential pattern is consistent with the ongoing, westward propagation of the closure of the Transcaucasian depression. In fact, East of the study area, the tectonic units of the Greater Caucasus and the Lesser Caucasus came already into contact after the Neogene closure of the intermontane depression.

4.3. Active tectonics and seismic hazard

The presence of folds and faults affecting Quaternary deposits and the diffuse seismicity testify to the presence of active tectonics in the studied area. The presence of several villages and, above all, of the Enguri hydroelectrical plant, pose a serious concern for geohazards. The 271-m-high Enguri dam, the 15-km-long artificial water reservoir, and the associated installations represent the most important facility of the country for energy production.

Although from the point of view of the general geomorphology of the area it appears that the southern front of the Greater Caucasus is the most prominent feature, in reality our data do not suggest the presence of an outcropping major fault here. The main fault responsible for the development of the structural flexure here is represented by the north-dipping blind thrust. This thrust allows the southward motions of this sector of the Caucasus and should accommodate most of the N-S shortening, also because, along the opposite northern front of the Caucasus, no major active faults have been detected (Reilinger et al., 2006; Avagyan et al., 2010; Tsereteli et al., 2016). In correspondence of the Enguri hydroelectrical scheme, the blind thrust is located at a depth of 4–9 km and due to its gentle dip, it maintains a shallow position below all the area of the Rioni Basin uplift; the hypocentre of a possible future earthquake might occur at any place along this thrust and, due to its shallow depth, a dissipation of the seismic energy will not be possible.

Two possible surface traces of active faults have been identified: one is located along the western border of the uplifted area and passes near Zugdidi town (Fig. 10). This fault has been imaged also on the seismic reflection sections and represents the emersion of the main thrust in the form of a splay fault (Fig. 15). This fault should

have been responsible for the 1614 Tsaishi earthquake that destroyed the nearby villages. Anyway, the seismic sections indicate the presence of a further thrust slice located further south, which represents the real frontal reverse fault of the embricated system.

The other surface fault trace corresponds to the E-W-striking back-thrust; also this slip plane is shallow because it should be connected with the main thrust plane. An earthquake here might occur with a focal depth in the order of less than 9 km.

The shallow depth of the main fault planes, the wealth of evidence of active tectonics in the area, and the position of these structures at the front of the contractional system of the Greater Caucasus, point to the need to devote more efforts to studying this area in terms of seismic hazard and risk assessment.

5. Conclusions

New field geological, geomorphological and structural data have been integrated with seismological data and seismic reflection sections in order to understand the geometry, kinematics and evolution of part of the Rioni Basin, located between the Greater and Lesser Caucasus in Georgia.

We confirm that marine and continental deposits of Cretaceous-Neogene age have been locally uplifted since the end of the Miocene. The area of uplift is of 1300 km^2, and Plio-Quaternary river deposits have been uplifted up to 200 m above the surrounding plane. The border of this area has been affected by the development of south-vergent asymmetrical folds and strike-slip faults, as already suggested by Banks et al. (1997) and Philip et al. (1989).

Some of these folds have a left-stepping en-échelon geometry and our new microtectonic data indicate rotation of the greatest principal stress σ_1. We thus suggest simple shear deformation linked with the southward propagation of tectonic blocks respect to the main Greater Caucasus front. In the interiors of the uplifted area, there are gentle symmetrical folds and one main recent, south-dipping reverse fault, corresponding to a backthrust.

A wealth of morpho-structural evidence, the tilting of some Quaternary strata, the offset of Quaternary alluvial deposits, and the presence of crustal seismic activity, indicate that compressional tectonics is still active.

The combination of these data with seismic reflection sections shows that inversion tectonics took place through a series of north-dipping blind main thrusts along the frontal part of a ramp-and-flat structure that becomes deeper below the Greater Caucasus. Contraction and uplift developed at a higher rate in the eastern part of the study area, in agreement with the westward ongoing propagation of the closure of the Transcaucasian depression.

Acknowledgments

We acknowledge suggestions on an earlier version of the manuscript by Gulam Babayev and an anonymous reviewer. Federico Pasquarè Mariotto is acknowledged for English review. This study has been carried out in the framework of the NATO project SfP G4934 “Georgia Hydropower Security”, of the International Lithosphere Program - Task Force II, and of the European Space Agency project n.32309 “Active tectonics and seismic hazard of southwest Caucasus by remotely-sensed and seismological data” that provided the satellite data (Leader A. Tibaldi). Seismic sections were kindly made available by the State Oil and Gas Agency of Georgia.

References

Adamia, Sh, Gujabidze, G., 2004. Geological Map of Georgia, 1:500,000 Scale. Georgian Department of Geology (ISTC Project).

Adamia, S.A., Zakariadze, G.S., Lordkipanidze, M.B., 1974. Evolution of an ancient active continental margin, Caucasus, as an example. Geotectonics 4, 88–103.

Adamia, Sh, Lordkipanidze, M.B., Zakariadze, G.S., 1977. Evolution of an active continental margins exemplified by the alpine history of the Caucasus. Tectonophysics 40, 183–199.

Adamia, Sh, Chkhotua, T., Kekelia, M., Lordkipanidze, M., Shavishvili, I., Zakariadze, G., 1981. Tectonics of Caucasus and adjoining regions: implications for the evolution of the Tethys ocean. J. Struct. Geol. 3, 437–447.

Adamia, Sh, Alania, V., Chabukiani, A., Chichua, G., Enukidze, O., Sadradze, N., 2010. Evolution of the late Cenozoic basins of Georgia (SW Caucasus): a review. In: Sosson, M., Kaymakçı, N., Stephenson, R., Bergerat, F. (Eds.), Sedimentary Basin Tectonics from the Black Sea and Caucasus to the Arabian Platform, vol. 340. Geological Society of London, pp. 239–259. Special Publication.

Adamia, Sh, Zakariadze, G., Chkhotua, T., Chabukiani, A., Sadradze, N., Tsereteli, N., Gventsadze, A., 2011a. Geology of the Caucasus: a review. Turk. J. Earth Sci. 20, 489–544.

Adamia, Sh, Alania, V., Chagelishvili, R., Chabukiani, A., Enukidze, O., Jaoshvili, G., Razmadze, A., Sadradze, N., 2011b. Tectonic setting of Georgia (Caucasus). In: 3rd International Symposium on the Geology of the Black Sea Region 1-10 October 2011, Bucharest, Romania, vol. 17, pp. 11–13. Abstracts Supplement to GEO-ECO-MARINA.

Adamia, Sh, Alania, V., Tsereteli, N., Varazanashvili, O., Sadradze, N., Lursmanashvili, N., Gventsadze, A., 2017. Post-collisional tectonics and seismicity of Georgia. In: Tectonic Evolution and Seismicity of South-west Asia. Geological Society of America (GSA). Special Paper (in press).

Alania, V., Chabukiani, A., Chagelishvili, R., Enukidze, O., Gogrichiani, K., Razmadze, A., Tsereteli, N., 2016. Growth structures, piggyback basins and growth strata of Georgian part of kura foreland fold and thrust belt: implication for Late Alpine kinematic evolution. In: Sosson, M., Stephenson, R., Adamia, Sh (Eds.), Tectonic Evolution of the Eastern Black Sea and Caucasus, 428. Geological Society of London. http://dx.doi.org/10.1144/SP428.5. Special Publications.

Albino, I., Cavazza, W., Zattin, M., Okay, A., Adamia, Sh, Sadradze, N., 2014. Far-field tectonic effects of the Arabia–Eurasia collision and the inception of the north Anatolian Fault system. Geol. Mag. 151, 372–379.

Allen, M., Jackson, J., Walker, R., 2004. Late Cenozoic reorganization of the Arabia-Eurasia collision and the comparison of short-term and long-term deformation rates. Tectonics 23, 16. http://dx.doi.org/10.1029/2003TC001530.

Angelier, J., 1990. Inversion of field data in fault tectonics to obtain the regional stress—III. A new rapid direct inversion method by analytical means. Geophys. J. Int. 103 (2), 363–376.

Avagyan, A., Sosson, M., Karakhanian, A., Philip, H., Rebai, S., Rolland, Y., Melkonyan, R., Davtyan, V., 2010. Recent tectonic stress evolution in the Lesser Caucasus and adjacent regions. In: Sosson, M., Kaymakci, N., Stephenson, R.A., Bergerat, F., Starostenko, V. (Eds.), Sedimentary Basin Tectonics from the Black Sea and Caucasus to the Arabian Platform, vol. 340. Geological Society, London, pp. 393–408. http://dx.doi.org/10.1144/SP340.17 0305-8719/10. Special Publications.

Avdeev, B., Niemi, N.A., 2011. Rapid Pliocene exhumation of the central greater Caucasus constrained by low-temperature thermochronometry. Tectonics 30, TC2009. http://dx.doi.org/10.1029/2010TC002808.

Banks, C., Robinson, A., Williams, M., 1997. Structure and regional tectonics of the Achara-Trialeti fold belt and the adjacent Rioni and Kartli foreland basins. Republic of Georgia. In: Robinson, A.G. (Ed.), Regional and Petroleum Geology of the Black Sea and Surrounding Region, 68. American Association of Petroleum Geologists Memoir, pp. 331–336.

Cloetingh, S., Spadini, G., Van Wees, J.D., Beekman, F., 2003. Thermo-mechanical modelling of the Black Sea Basin (de)formation. Sediment. Geol. 156, 169–184.

Devlin, W.J., Cogswel, J.M., Gaskins, G.M., Isaken, G.H., Picther, D.M., Puls, D.P., Stanely, K.O., Wall, G.R.T., 1999. South Caspian basin: young, cool, and full of promise. GSA Today 9 (7), 1–9.

Dercourt, J., Zonenschain, L.P., Ricou, L.E., Kazmin, V.G., Le Pichon, X., Knipper, A.L., Grandjacquet, C., Sbortshikov, I.M., Geyssant, J., Lepvir, C., Pechersky, D.H., Boulin, J., Sibuet, J.C., Savostin, L.A., Sorokhtin, O., Westphal, M., Bazhenov, M.L., Lauer, J.P., Biju-Duval, B., 1986. Geological evolution of the Tethys belt from the Atlantic to the Pamirs since the Lias. Tectonophysics 123, 241–315.

Ferrari, L., Tibaldi, A., Brizzolara, L., Maffioli, A., 1990. Eocene simple shear and Pliocene pure shear folding in the central-eastern Algerian Atlas. Terra Nova 2, 653–660.

Finetti, I., Bricchi, G., Del Ben, A., Pipan, M., Xuan, Z., 1988. Geophysical study of the black sea. Boll. Geofis. Appl. 30, 197–324.

Forte, A., Cowgill, E., Bernardin, T., Kreylos, O., Hamann, B., 2010. Late Cenozoic deformation of Kura fold-thrust belt, southern greater Caucasus. Geol. Soc. Am. Bull. 122, 465–486.

Forte, A., Cowgill, E., Whipple, K.X., 2014. Transition from a singly vergent to doubly vergent wedge in a young orogen: the Greater Caucasus. Tectonics 33, 2077–2101.

Heidbach, O., 2009. Spatial and Temporal Variability of the Contemporary Crustal Stress Pattern of the Earth. Doctoral dissertation. Zugl.: Karlsruhe, Univ., Habilitationsschr.

Jones, R.W., Simmons, M.D., 1997. A review of the stratigraphy of eastern Paratethys (Oligocene-Holocene), with particular emphasis on the black sea. In: Robinson, A.G. (Ed.), Regional and Petroleum Geology of the Black Sea and Surrounding Region, vol. 68. American Association of Petroleum Geologists Memoir, pp. 39–52.

Kadirov, F.A., Gadirov, A.G., Babayev, G.R., Agayeva, S.T., Mammadov, S.K., Garagezova, N.R., Safarov, R.T., 2013. Seismic zoning of the southern slope of Greater Caucasus from the fractal parameters of earthquakes, stress state and GPS velocities. Izv. Phys. Solid Earth 49 (4), 554–562 (in Russian).

Khain, V.E., 1974. Structure and main stages in the tectono-magmatic development of the Caucasus: an attempt at geodynamic interpretation. Am. J. Sci. 274, 16–23.

Khriachtchevskaia, O., Stovba, S., Stephenson, R., 2010. Cretaceous-Neogene tectonic evolution of the northern margin of the Black Sea from seismic reflection data and tectonic subsidence analysis. In: Sosson, M., Kaymakci, N., Stephenson, R., Bergerat, F., Starostenko, V. (Eds.), Sedimentary Basin Tectonics from the Black Sea and Caucasus to the Arabian Platform, vol. 340. Geol. Soc. London, pp. 137–157. Spec. Publ.

Koçyiğit, A., Yılmaz, A., Adamia, S., Kuloshvili, S., 2001. Neotectonics of east Anatolia plateau (Turkey) and Lesser Caucasus: implication for transition from thrusting to strike-slip faulting. Geodin. Acta 14, 177–195.

Koronovskii, N.V., Demina, L.I., 1999. Collision stage of the evolution of the Caucasian sector of the Alpine fold belt: geodynamics and magmatism. Geotectonics 33, 102–118.

Letouzey, J., Biju-Duval, B., Dorkel, A., Gonnard, R., Kritchev, K., Montadert, L., Sungurlu, O., 1977. The Black Sea: a marginal basin; geophysical and geological data. In: Biju-Duval, B., Montadert, L. (Eds.), International Symposium on the Structural History of the Mediterranean Basins. Technip, Paris, pp. 363–376.

McClay, K.R., 2011. Introduction to thrust fault-related folding. In: McClay, K.R., Shaw, J., Suppe, J. (Eds.), Thrust Fault-related Folding, vol. 94. AAPG Mem, pp. 1–19.

McClusky, S., Balassanian, S.A., Demir, C., Ergintav, S., Georgiev, I., Gurkan, O., Hamburger, M., Hurst, K., Kahle, H., Kastens, K., Kekelidze, G., King, R., Kotzev, V., Lenk, O., Mahmoud, S., Mishin, A., Nadariya, M., Ouzounis, A., Paradisssis, D., Peter, Y., Prilepin, M., Reilinger, R., Sanli, I., Seeger, H., Tealeb, A., Toksoz, M.N., Veis, G., 2000. Global Positioning System constraints on plate kinematics and dynamics in the eastern Mediterranean and Caucasus. J. Geophys. Res. Solid Earth 105 (B3), 5695–5719.

McQuarrie, N., Stock, J.M., Verdel, C., Wernicke, B.P., 2003. Cenozoic evolution of Neotethys and implications for the causes of plate motions. Geophys. Res. Lett. 30 http://dx.doi.org/10.1029/2003GL017992.

Mitra, S., 1990. Fault-propagation folds: geometry and kinematic evolution, and hydrocarbon traps. AAPG Bull. 74, 921–945.

Mosar, J., Kangarli, T., Bochud, M., Glasmacher, U.A., Rast, A., Brunet, M., Sosson, M., 2010. Cenozoic–recent tectonics and uplift in the greater Caucasus: a perspective from Azerbaijan. In: Sosson, M., Kaymakçı, N., Stephenson, R., Bergerat, F. (Eds.), Sedimentary Basin Tectonics from the Black Sea and Caucasus to the Arabian Platform, vol. 340. Geological Society of London, pp. 261–279. Special Publication.

Okay, A.I., Sengör, A.M.C., Görür, N., 1994. Kinematic history of the opening of the Black Sea and its effect on the surrounding regions. Geology 22, 267–270.

Okay, A.I., Sunal, G., Sherlock, S., Altıner, D., Tüysüz, O., Kylander-Clark, A.R.C., Aygül, M., 2013. Early Cretaceous sedimentation and orogeny on the active margin of Eurasia: southern Central Pontides, Turkey. Tectonics 32, 1247–1271.

Pasquaré, F., Tormey, D., Vezzoli, L., Okrostsvaridze, A., Tutberidze, B., 2011. Mitigating the consequences of extreme events on strategic facilities: evaluation of volcanic and seismic risk affecting the Caspian oil and gas pipelines in the Republic of Georgia. J. Environ. Manag. 92, 1774–1782.

Philip, H., Cisternas, A., Gvishiani, A., Gorshkov, A., 1989. The Caucasus: an actual example of the initial stages of continental collision. Tectonophysics 161, 1–21.

Rebai, S., Philip, H., Dorbath, L., Borissoff, B., Haessler, H., Cisternas, A., 1993. Active tectonics in the Lesser Caucasus: coexistence of compressive and extensional structures. Tectonics 12 (5), 1089–1114.

Reilinger, R.E., McClusky, S.C., Oral, M.B., King, R.W., Toksoz, M.N., Barka, A.A., Kinik, I., Lenk, O., Sanli, I., 1997. Global positioning system measurements of present-day crustal movements in the Arabia-Africa-Eurasia plate collision zone. J. Geophys. Res. 102 (5), 9983–9999.

Reilinger, R.E., McClusky, S.C., Vernant, P., Lawrence, S., Ergintav, S., Cakmak, R., Ozener, H., Kadirov, F., Guliev, I., Stepanian, R., Nadariya, M., Hahubia, G., Mahmoud, S., Sakr, K., Arrajehi, A., Paradissis, D., Al-Aydrus, A., Prilepin, M., Guseva, T., Evren, E., Dmirotsa, A., Filikov, S.V., Gomez, F., Al-Ghazzi, R., Karam, G., 2006. GPS constraints on continental deformation in the Africa-Arabia-Eurasia continental collision zone and implications for the dynamics of plate interactions. J. Geophys. Res. 111 (B5) http://dx.doi.org/10.1029/2005JB004051.

Robinson, A.G., Rudat, J.H., Banks, C.J., Wiles, R.L.F., 1996. Petroleum geology of the Black Sea. Mar. Pet. Geol. 13, 195–223.

Sasvári, Á., Baharev, A., 2014. SG2PS (Structural Geology to Postscript Converter)–A graphical solution for brittle structural data evaluation and paleostress calculation. Comput. Geosci. 66, 81–93.

Spadini, G., Robinson, A., Cloeting, S., 1996. Western v. eastern Black Sea tectonic evolution: pre-rift lithosphere controls on basin formation. Tectonophysics 266, 139–154.

Sosson, M., Rolland, Y., Danelian, T., Muller, C., Melkonyan, R., Adamia, S., Kangarli, T., Avagyan, A., Galoyan, G., 2010. Subductions, obduction and collision in the Lesser Caucasus (Armenia Azerbaijan, Georgia), new insights. In: Sosson, M., Kaymakci, N., Stephanson, R., Bergarat, F., Starostenko, V. (Eds.), Sedimentary Basin Tectonics from the Black Sea and Caucasus to the Arabian Platform, vol. 340. Geological Society of London, pp. 329–352. Special Publication.

Sosson, M., Adamia, Sh, Muller, C., Sadradze, N., Rolland, Y., Alania, V., Enukidze, O., Hassig, M., 2013. From greater to lesser Caucasus: new insights from surface and subsurface data along a N-S trending transect (Georgia): thick-skin versus thin-skin tectonics. Darius News 3, 5–7.

Sosson, M., Stephenson, R., Sheremet, Y., Rolland, Y., Adamia, Sh, Melkonian, R., Kangarli, T., Yegorova, T., Avagyan, A., Galoyan, G., Danelian, T., Hässig, M., Meijers, M., Müller, C., Sahakyan, L., Sadradze, N., Alania, V., Enukidze, O., Mosar, J., 2016. The eastern Black Sea-Caucasus region during Cretaceous: new evidence to constrain its tectonic evolution. Compte-Rendus Geosci. 348 (1), 23–32.

Stephenson, R.A., Schellart, W., 2010. The Black Sea back-arc basin: insights to its origin from geodynamic models of modern analogues. In: Sosson, M., Kaymakci, N., Stephenson, R.A., Bergerat, F., Starostenko, V. (Eds.), Sedimentary Basin Tectonics from the Black Sea and Caucasus to the Arabian Platform, vol. 340. Geol. Soc. London, pp. 11–21. Spec. Publ.

Spang, J.H., 1972. Numerical method for dynamic analysis of calcite twin lamellae. Geol. Soc. Am. Bull. 83 (2), 467–471.

Suppe, J., 1983. Geometry and kinematics of fault-bend folding. Am. J. Sci. 283, 684–721.

Suppe, J., Medwedeff, D.A., 1990. Geometry and kinematics of fault-propagation folding. Eclogae Geol. Helv. 83, 409–454.

Tan, O., Taymaz, T., 2006. Active tectonic of the Caucasus: earthquake source mechanisms and rupture histories obtained from inversion of teleseismic body waves. Geol. Soc. Am. 409, 531–578 special paper.

Tsereteli, N., Tibaldi, A., Alania, V., Gventsadse, A., Enukidze, O., Varazanashvili, O., Müller, B.I.R., 2016. Active tectonics of central-western Caucasus, Georgia. Tectonophysics 691, 328–344.

Turner, F.J., 1953. Nature and dynamic interpretation of deformation lamellae in calcite of three marbles. Am. J. Sci. 251, 276–298.

Varazanashvili, O., Tsereteli, N., Tsereteli, E., 2011. Historical Earthquakes in Georgia (Up to 1900): Source Analysis and Catalogue Compilation. Monograph, Pub. Hause MVP, Tbilisi, pp. 39–40.

Vincent, S.J., Allen, M., Ismail-Zadeh, A., Flecker, R., Foland, K., Simmons, M., 2005. Insights from the Talysh of Azerbaijan into the Paleogene evolution of the south Caspian region. Geol. Soc. Am. Bull. 117 (11/12), 1513–1533.

Vincent, S.J., Morton, A.C., Carter, A., Gibbs, S., Teimuraz, G.B., 2007. Oligocene uplift of the western greater Caucasus: an effect of initial Arabia-Eurasia collision. Terra Nova 19, 160–166.

Vincent, S.J., Carter, A., Lavrishchev, V.A., Price, S.P., Barabadze, T.G., Hovius, N., 2011. The exhumation of the western Greater Caucasus: a thermochronometric study. Geol. Mag. 148, 1–21.

Westaway, R., 1994. Present-day kinematics of the middle east and eastern Mediterranean. J. Geophys. Res. 99, 12,071–12,090.

Williams, G., Chapman, T., 1983. Strains developed in the hangingwalls of thrusts due to their slip/propagation rate: a dislocation model. J. Struct. Geol. 5, 563–571.

Yegorova, T., Gobarenko, E., 2010. In: Sosson, M., Kaymakci, N., Stephenson, R.A., Bergerat, F., Starostenko, V. (Eds.), Structure of the Earth's Crust and Upper Mantle of the West- and East-black Sea Basins Revealed from Geophysical Data and its Tectonic Implications, vol. 340. Geol. Soc. of London, pp. 23–42. Spec. Publ.

Zakariadze, G., Dilek, Y., Adamia, S., Oberhansli, R., Karpenko, S., Bazylev, B., Soloveva, N., 2007. Geochemistry and geochronology of the Neoproterozoic Pan-African Transcaucasian massif (Republic of Georgia) and implications for island-arc evolution of the late Precambrian Arabian–Nubian Shield. Gondwana Res. 11, 92–108.

Zoback, M.L., 1992. First- and second-order patterns of stress in the lithosphere: the world stress map project. J. Geophys. Res. 97 (B8), 11,703–11,728.

Zonenshain, L.P., Le Pichon, X., 1986. Deep basins of the Black Sea and Caspian Sea as remnants of Mesozoic back-arc basins. Tectonophysics 123, 181–211.